



<http://www.diva-portal.org>

Postprint

This is the accepted version of a paper published in *Physics of fluids*. This paper has been peer-reviewed but does not include the final publisher proof-corrections or journal pagination.

Citation for the original published paper (version of record):

Abidakun, O., Adebisi, A., Valiev, D., Akkerman, V. (2021)

Impacts of fuel nonequidiffusivity on premixed flame propagation in channels with open ends

Physics of fluids, 33: 013604

<https://doi.org/10.1063/5.0019152>

Access to the published version may require subscription.

N.B. When citing this work, cite the original published paper.

This article may be downloaded for personal use only. Any other use requires prior permission of the author and AIP Publishing. This article appeared in O. Abidakun et al., *Phys. Fluids* 33, 013604 (2021) and may be found at <https://doi.org/10.1063/5.0019152>.

Permanent link to this version:

<http://urn.kb.se/resolve?urn=urn:nbn:se:umu:diva-178870>

Impacts of Fuel Nonequidiffusivity on Premixed Flame Propagation in Channels with Open Ends

Olatunde Abidakun¹, Abdulafeez Adebiyi¹, Damir Valiev^{2,3}, Vyacheslav Akkerman^{1,*}

¹Center for Innovation in Gas Research and Utilization (CIGRU)
Department of Mechanical and Aerospace Engineering, West Virginia University
Morgantown, West Virginia, 26506, USA

²Center for Combustion Energy, Key Laboratory for Thermal Science and Power Engineering of the Ministry of Education of China, Department of Energy and Power Engineering, Tsinghua University, Beijing, 100084, China

³Department of Applied Physics and Electronics, Umeå University, 901 87 Umeå, Sweden

*Corresponding Author Email: Vyacheslav.Akkerman@mail.wvu.edu

Abstract

The present study scrutinizes premixed flame dynamics in micro-channels, thereby shedding the light on advanced miniature micro-combustion technologies. While equidiffusive burning (when the Lewis number $Le = 1$) is a conventional approach adopted in numerous theoretical studies, real premixed flames are typically non-equidiffusive ($Le \neq 1$), which leads to intriguing effects, such as the diffusional-thermal instability. The equidiffusive computational study [Akkerman *et al.*, Combust. Flame 145 (2006) 675] reported regular oscillations of premixed flames spreading in channels having nonslip walls and open extremes. Here, this investigation is extended to non-equidiffusive combustion in order to systematically study the impact of the Lewis number on the flame in this geometry. The analysis is performed by means of computational simulations of the reacting flow equations with fully-compressible hydrodynamics and one-step Arrhenius chemical kinetics in channels with adiabatic and isothermal walls. In the adiabatic channels, which are the main case of study, it is found that the flames oscillate at low Lewis numbers, with the oscillation frequency decreasing with Le ; while for the $Le > 1$ flames, a tendency to steady flame propagation is observed. The oscillation parameters also depend on the thermal expansion ratio and the channel width, though the impacts are rather quantitative than qualitative. The analysis is subsequently extended to the isothermal channels. It is shown that the role of heat losses to the walls is important and may potentially dominate over that of the Lewis number. At the same time, the impact of Le on burning in the isothermal channels is qualitatively weaker than that in the adiabatic channels.

Keywords: Lewis number; adiabatic walls; isothermal walls; premixed flames; flame oscillations; open channels; computational simulations.

Nomenclature

| | |
|--------------------------------------|---|
| C_v | Specific heat at constant volume |
| C_p | Specific heat at constant pressure |
| E_a | Activation energy |
| $e = QY + C_v T$ | Specific internal energy |
| $h = QY + C_p T$ | Specific enthalpy |
| $Le = Sc/Pr$ | Lewis number |
| $L_f \equiv \zeta_f / \rho_f S_L Pr$ | Flame thickness |
| m | Molecular weight |
| \mathbf{n} | Normal vector |
| Pr | Prandtl number |
| P | Pressure |
| Q | Specific energy release in the reaction |
| q_i | Energy diffusion vector |
| R_p | Universal gas constant |
| R | Channel half-width |
| Sc | Schmidt number |
| S_L | Unstretched laminar burning velocity |
| T | Temperature |
| t | Time |
| U_w | Instantaneous total burning velocity |
| U_{tip} | Flame tip velocity |
| \mathbf{u} | Velocity vector |

| | |
|-----------|---------------------------------------|
| u_i | Velocity i -component, $i = (x, z)$ |
| x | Radial direction |
| Y | Mass fraction of the fuel mixture |
| Z_{tip} | Flame tip position |
| z | Axial direction |

Greek letters

| | |
|---------------------------------|----------------------------|
| $\gamma_{i,j}$ | Stress tensor |
| ρ | Density |
| $\Theta \equiv \rho_f / \rho_b$ | Thermal expansion ratio |
| ν | Kinematic viscosity |
| $\zeta = \rho\nu$ | Dynamic viscosity |
| τ_R | Constant of time dimension |

Subscripts

| | |
|-------|------------------|
| f | Fuel mixture |
| b | Burnt matter |
| tip | Flame tip |
| DL | Darrieus-Landau |
| x | Radial direction |
| z | Axial direction |

1. Introduction

Emerging development of miniature, portable devices (micro-satellite thrusters, micro-chemical reactors and sensors, etc.) requires efficient and reliable systems powered by the micro-combustion technologies. The latter depend on the deep physical understanding of the heat and momentum transfer processes occurring in micro- and mesoscale combustors, with micro-channels being ones of the simplest examples of such micro-combustors. It is noted, in this this respect, that self-sustenance of flame propagation in channels is largely dependent on continuous diffusion of mass and heat upstream and downstream of the flame front, which is characterized by the Lewis number, Le , defined as the thermal-to-mass diffusivities ratio¹. In numerous theoretical studies on flame propagation in channels, these diffusion processes are considered to occur at equal rates, signifying a conventional assumption of equidiffusive combustion, i.e. of the unity Lewis number, $Le = 1$. However, differential diffusion of heat and mass usually occurs in the practical reality such that the real flames are typically non-equidiffusive, having $Le \neq 1$ and, thereby, experiencing various phenomena including an onset of the diffusional-thermal instability of the flame front. The Lewis number has generally been found to affect the behavior of flames in many ways. Its impacts on heat and mass transfer², vorticity³⁻⁵ and enstrophy⁵, scalar and surface density transport^{6,7}, flame bifurcation and extinction⁸, stretched flame speeds⁹ and generation of primary acoustic instability¹⁰ have been reported, with numerical simulations particularly focusing on lean-premixed flames^{11,12}.

Other studies¹³⁻¹⁸ have identified that the variations of Le cause changes in the dynamics and morphology of premixed flames in channels. It is noted that such flame dynamics/morphology and the impact of Le on it depends, conceptually, on the channel geometry. For instance, in a “semi-open” channels (one channel end is closed, while the other is open), with or without obstructions, a flame is known to accelerate from the closed end towards the open one, and the changes in Le

are reported to either facilitate or moderate acceleration^{14,17}. In the “opposite” geometry of a flame propagating from the open end to the closed one, flame-acoustic coupling occurs, generally leading to profound flame oscillations, with a decrease in Le facilitating these oscillations¹⁸ (note that the definition of the Lewis number in Ref. 18 is inverse to that employed the present work). At certain conditions, such flame-acoustic coupling may result in a strong flame-acoustic resonance, violent folding of the flame front and even its turbulization¹⁹. In such a configuration of flame propagation towards the closed end, the oscillatory premixed flames have also been observed in a Hele-Shaw cell (see, for instance, the recent experimental work²⁰ and numerous references therein).

Unlike the previous studies¹³⁻¹⁸, the present work is devoted to channels with both extremes open. It is in this geometry that a new mode of flame propagation has been identified: namely, intrinsic oscillations of the flame front²¹ (being different from an accelerating regime observed for semi-open channels). Specifically, according to the numerical simulations²¹, spreading through a two-dimensional (2D) channel with adiabatic, nonslip walls and both extremes open, a flame front acquires a concave shape and oscillates, with oscillation parameters (such as frequency, amplitude) depending on a characteristic width of the channel. Other computational studies^{22,23} also identified similar flame oscillations in micro-channels. It is noted, in this respect, that only equidiffusive ($Le = 1$) flames were studied in Ref. 21. Consequently, it is of interest how the flame behavior in such a configuration would be influenced by any deviations of the Lewis number from unity.

This concern is addressed in the present work, where the impacts of varying Le , caused by differential diffusion of mass and heat, on the dynamics and morphology of flames in 2D channels with both extremes open is studied. The systematic approach involves computational simulations of the reacting flow equations, with fully-compressible hydrodynamics and one-step Arrhenius chemical kinetics. It is specifically investigated how changes in Le (in conjunction with variations

in the thermal expansion ratio $\Theta \equiv \rho_f/\rho_b$, the wall thermal boundary conditions, and the scaled channel width) impact the position of the flame tip and the burning rate. In the adiabatic channels, the flames are found to oscillate at low Lewis numbers, with the oscillation frequency decreasing with Le . In contrast, the $Le > 1$ flames experience a tendency to steady propagation. Also, while the majority of the simulation runs of the present work employed the adiabatic channel wall condition, for comparison, isothermal channels were also considered and discussed. As a result, heat losses to the walls are shown to be an important factor controlling the combustion process, with the flame shape being qualitatively different from that in the adiabatic channels. At the same time, the impact of Le in the isothermal channels is weaker than that in the adiabatic ones.

2. Description of the Numerical Simulations

Computational simulations of the hydrodynamic and combustion equations were performed. In the 2D Cartesian geometry, employed in the present work, the system of governing equations reads:

$$\frac{\partial}{\partial t} \rho + \frac{\partial}{\partial x_i} (\rho u_i) = 0, \quad (1)$$

$$\frac{\partial}{\partial t} (\rho u_i) + \frac{\partial}{\partial x_j} (\rho u_i u_j + \delta_{ij} P - \gamma_{i,j}) = 0, \quad (2)$$

$$\frac{\partial}{\partial t} \left(\rho e + \frac{1}{2} \rho u_i u_i \right) + \frac{\partial}{\partial x_i} \left(\rho u_i h + \frac{1}{2} \rho u_i u_j u_j + q_i - u_j \gamma_{i,j} \right) = 0, \quad (3)$$

$$\frac{\partial}{\partial t} (\rho Y) + \frac{\partial}{\partial x_i} \left(\rho u_i Y - \frac{\zeta}{S_c} \frac{\partial Y}{\partial x_i} \right) = -\frac{\rho Y}{\tau_R} \exp(-E_a / R_p T), \quad (4)$$

where Y is the mass fraction of the fuel mixture, $e = QY + C_v T$ and $h = QY + C_p T$ the specific internal energy and enthalpy, respectively, $Q = C_p T_f (\Theta - 1)$ the energy release in the reaction, and C_v , C_p the specific heats at constant volume and pressure. Both unburned and burnt matters are assumed to be two-atomic ideal gases of the same molecular weight $m = 2.9 \times 10^{-2} \text{ kg/mol}$, with $C_v = 5R_p/2m$, $C_p = 7R_p/2m$, the universal gas constant $R_p = 8.314 \text{ J/(mol} \cdot \text{K)}$, and the

equation of state $P = \rho R_p T / m$. We employ the initial fuel temperature, $T_f = 300$ K, pressure $P_f = 1$ bar, and density $\rho_f = 1.16$ kg/m³. The stress tensor $\gamma_{i,j}$ and the energy diffusion vector q_i read

$$\gamma_{i,j} = \zeta \left(\frac{\partial u_i}{\partial x_j} + \frac{\partial u_j}{\partial x_i} - \frac{2}{3} \frac{\partial u_k}{\partial x_k} \delta_{i,j} \right), \quad q_i = -\zeta \left(\frac{C_p}{\text{Pr}} \frac{\partial T}{\partial x_i} + \frac{Q}{\text{Sc}} \frac{\partial Y}{\partial x_i} \right), \quad (5)$$

where $\zeta = \rho \nu$ is the dynamic viscosity having a value of 1.7×10^{-5} kg/(m · s) in the fuel mixture, Pr and Sc are the Prandtl and Schmidt numbers, respectively. Their ratio is the Lewis number, $Le = \text{Sc}/\text{Pr}$. In the present work, it is varied in the range $0.2 \leq Le \leq 2.0$ by keeping $\text{Pr} = 1 = \text{const}$ and adjusting Sc accordingly. Equation (4) describes an irreversible one-step Arrhenius reaction of the first order, with the activation energy E_a and a constant of time dimension τ_R . A conventional unit of velocity dimension is the unstretched laminar flame velocity S_L . In the present work, $S_L = 34.7$ cm/s, being 10^3 times smaller than the initial speed of sound in this fuel mixture, $c_0 = 347$ m/s such that the hydrodynamics is almost incompressible at the initial stage of burning. A useful unit of length dimension is the thermal flame thickness, which is conventionally defined as $L_f \equiv \zeta_f / \rho_f S_L \text{Pr} = 4.22 \times 10^{-5}$ m. We therefore measure the channel width in terms of L_f .

The set of Eqs. (1) – (5) has been solved by means of a fully-compressible Navier–Stokes code, which is adapted for parallel computations and employs an adaptive mesh. Accurate and robust, this code has been successfully utilized in numerous aero-acoustic²⁴ and combustion^{25–28} applications. The numerical approach is based on a cell-centered, finite-volume numerical scheme, which is of the 2nd-order accuracy in time and the 4th-order in space for the convective terms, and of the 2nd-order in space for the diffusive terms. Specifically, the code employs all the balance equations (1) – (4) in a unified form²⁵

$$\frac{\partial G}{\partial t} + \frac{\partial E_G}{\partial z} + \frac{\partial F_G}{\partial x} = H_G, \quad (6)$$

where G stands for any of the variables ρ , ρu_x , ρu_z , ρY_F and e , while E_G and F_G designate the related axial and radial fluxes, respectively, and H_G is the source term. The spatial discretization is obtained by integrating any of the balance equations (1) – (4) in the form (6) over a given grid cell. More details about the numerical method are available, for instance, in Refs. [14,17,21,27,28](#).

In the present work, we consider a premixed flame front propagating in a long 2D channel of half-width $R/L_f = 10, 20, 30$ and the thermal expansion ratio $\Theta \equiv \rho_f/\rho_b = 5, 8, 10$. The surface of the channel wall is nonslip $\mathbf{u} = 0$, and either adiabatic, $\mathbf{n} \cdot \nabla T = 0$, or isothermal, $T = 300$ K. The nonreflecting boundary conditions with the velocity field $(u_x, u_y) = 0$ are employed at both ends of a channel to prevent the reflection of the sound waves and weak shocks. The initial flame structure is imitated by the Zeldovich-Frank-Kamenetskii (ZFK) solution for a planar flame front²¹ initiated at the distance of $50 L_f$ from the left end of the channel. The flames are characterized by monitoring the evolution of the flame tip position as well as that of the instantaneous burning rate U_w given by¹⁸

$$U_w = \frac{1}{2R\rho_f} \int \frac{\rho Y}{\tau_R} \exp\left(-\frac{E_A}{R_p T}\right) dx dz. \quad (7)$$

After carrying out adequate resolution tests, using standard procedure adopted in some of our previous works^{14,17,27,28}, a grid size of $0.2 L_f$ is found to fully resolve the flame front and optimize resource utilization.

3. Results

The morphology of flames with various Lewis numbers, initiated as the ZFK solution and propagating through a channel with both ends open, presents some interesting features that can help in gaining understanding into the dynamics of such flames. Right after flame initiation, there is distortion of the flame front due to the impact of the thermal expansion and the nonslip wall.

The evolution of a flame in a channel of half-width $R = 10 L_f$ and thermal expansion ratio $\Theta = 5$ is shown in Fig. 1. For the $Le = 0.2$ flame, shown in Fig. 1a, it is revealed that the flame front becomes corrugated, showing concave shape with three wings, such that the center is behind the other segments. As the flame propagates, its segments close to the wall moves further into the premixture, while the central segments becomes deeper, causing formation of a cusp at the center of the channel, and thus promoting the flame surface area. This results in bifurcation, causing the unburnt fuel mixture to be entrapped between the flame segments, thereby further increasing the surface area of the flame front. The flame segments eventually collapse when the entrapped fuel is consumed. This process is repeated again because of the competing momenta of the burnt gas and the fuel mixture. Since both ends of the channel are open, the flow is not restricted in any direction and, therefore, this flow is distributed between the flows towards both exits. The cycle of cusp formation, flame bifurcation, and collapse of the flame segments continues, resulting in deceleration and acceleration of the flame tip. The flame tip is found to decelerate during formation of the cusp and bifurcation, and it accelerates during the collapse of the segments. Such an extent of the flame front distortion, observed for a flame with $Le = 0.2$, can be devoted to a thinner flame front, which make corrugation easier, and the increased flame stretch due to the diffusional-thermal instability²⁹. For the situation of $Le = 1$, Fig. 1b, the flame front is less distorted as compared with the $Le < 1$ flame. Here, the cusp formed in the flame front is not as deep as that in the case of $Le < 1$, and there is no flame bifurcation. Due to less distortion of the flame front, its surface area is lower and, therefore, the extent to which the flame would accelerate or decelerate is reduced. The $Le = 2$ flame in Fig. 1c shows a similar behavior to that of $Le = 1$; however, the cusp and, consequently, the flame surface area is slightly lower for $Le = 2$. Less distortion of the $Le \geq 1$

flames can be attributed to a thicker flame front at such Le , which makes the flame less susceptible to corrugation, in there is no diffusion-thermal instability in this case.

In a wider channel of half-width $R = 20 L_f$, Fig. 2, flame propagation still exhibits a similar trend to that of $R = 10 L_f$, especially at $Le \geq 1$. While the $Le = 0.2$ flame in Fig. 2a also shows a similar series of cusp formation, flame bifurcation, and collapse of flame segments, as discussed earlier for $R = 10 L_f$, the wider channel allows stronger corrugation of the flame front. The flame is almost divided into two halves along the centerline, before the collapse of the flame segments. is completed.

To describe the dynamics of a flame propagating through an open channel with adiabatic and non-slip walls, the plots of the scaled flame tip position Z_{tip}/R and scaled burning rate U_w/S_L versus the scaled time $\tau = tS_L/R$ for a channel of half-width $R = 10 L_f$ and a flame of thermal expansion ratio $\Theta = 5$ are shown in Figs. 3a and 3b, respectively. Both plots in Fig. 3 show that the flames oscillate as they propagate through the channels. The oscillations are however found to be much more prevalent for the $Le = 0.2$ flame, which can be devoted to the combustion instability inherent to low- Le flames. The oscillations observed here for the $Le = 0.2$ flame further confirm the implication of a trough formation and the subsequent collapse of the flame segments identified in Figs. 1a and 2a. We also mention in passing that the oscillation amplitude decreases as the flame propagates through the channel, signifying some reduction in the flame oscillations with distance.

For $Le = 1$ and 2, only minor oscillations are seen at the initial stage of flame propagation. The flame front is subsequently stabilized and propagates with a constant velocity as indicated by the plots of the scaled flame tip position Z_{tip}/R , Fig. 3a, and the scaled total burning rate U_w/S_L , Figs. 3b. It is important to mention here that for both equidiffusive ($Le = 1$) and non-equidiffusive ($Le \neq 1$) conditions, flame acceleration (observed in a semi-open channel for a flame ignited at a

closed end)¹⁶ is not observed here. This is due to the fact that the flow is not constrained to any direction when both channel extremes are open and, therefore, the fluid flow is distributed towards both ends. The resulting effect of this condition is that the opposing momenta of the burnt gas behind the flame and the fuel mixture ahead of the flame, more or less, balance each other, thereby preventing significant push from the burnt gas.

For a channel half-width increased to $20 L_f$, the plots for the time evolutions of the scaled flame position and burning rate in Figs. 4a and 4b, respectively, demonstrate that flame propagation through the channel preserves the oscillation regime. However, the flame oscillations are observed here to be of lower frequency as compared with that in the $R = 10 L_f$ channel. In such a wider channel as $R = 20 L_f$, the flame exhibits well defined oscillations when $Le \geq 1$, similar to the findings of Ref. 13. The difference in the flame behavior, caused by the changes in the channel width, can be attributed to the increased corrugation of the flame front in a wider channel.

Finally, it is emphasized that employment of *nonslip* walls was essential for this work. Indeed, if the wall were *slip* and adiabatic, then an initially planar, stable flame front would remain planar and would propagate with the constant velocity S_L with respect to the fuel mixture. This is typically the case for such narrow channels with slip walls. In practice, however, the channels are wider than those considered here, and the flame will eventually become unstable due to the onset of the intrinsic combustion instabilities. In fact, such a channel with slip walls has been the classical geometry to simulate the Darrieus-Landau (DL) instability^{25,26}, associated with the thermal expansion Θ , and the diffusional-thermal instability^{4,12}, associated with $Le < 1$.

In the present work, the situation is conceptually different because of the nonslip walls, which contribute to the formation of the curved flame front and play a key role in the flame dynamics and morphology. Due to the velocity gradient imposed by the nonslip wall condition, at different

channel widths, the flame front and the characteristics of flame propagation are different. For this reason, the channel width influences the oscillation frequency, even for a given Le . Overall, it looks as the flame oscillations are the result of the interplay between the effects of (i) nonslip walls, (ii) the DL instability, and (iii) the diffusional-thermal instability. The first two effects depend on R/L_f , so it is natural that the oscillation frequency also depends on R/L_f . Moreover, even for the same, fixed Le , the oscillation frequency depends on R/L_f because both the effects, of the nonslip walls and of the DL instability, exhibit such a dependence. In fact, the dependence of the oscillation frequency on the channel width follows the trend first established in the $Le = 1$ work²¹.

4. Discussion

We next discuss the effects of the thermal expansion ratio and thermal wall conditions (adiabatic or isothermal) on the flame dynamics in this geometry.

4a. Impact of thermal expansion

First, we keep the channel walls adiabatic, as in the previous section, and vary the expansion ratio Θ , which characterizes the density jump across the flame front. A higher level of the DL instability occurs for higher Θ . This is indicated in the temperature snapshots for the $\Theta = 10$ flames in a channel of $R = 10 L_f$ as shown in Fig. 5. The morphology of the flame front at this condition is qualitatively similar to that exhibited when $\Theta = 5$, with a stronger flame distortion experienced when $Le = 0.2$. The corrugation of the flame front and, consequently, the oscillations decrease as the Lewis number grows from $Le = 0.2$ to 2.

Figures 6 (a-c) present the scaled flame tip position, the scaled flame tip velocity as well as the scaled total burning rate, respectively, versus scaled time for the flames with a higher thermal expansion ratio, $\Theta = 10$. Figures 7 (a-c) are the counterparts of Figs. 6 (a-c) for $\Theta = 8$. It is seen that increasing the thermal expansion ratio from 5 to 8 and 10 does not produce any qualitative

effects on the flame dynamics, preserving the oscillating mode of the flame dynamics. However, minor quantitative differences in terms of the oscillation parameters are noticed. Another important finding is a damping effect of Le . It is observed that, as the Lewis number grows from 0.2 to 2, the amplitude of the flame oscillations decreases. The $Le < 1$ flames clearly exhibit oscillations with a decreasing amplitude and frequency, as Le approaches unity. Such a reduction in the oscillation parameters indicates the flame stability, which is promoted with an increase in Le .

The maximal scaled total burning rate attained by the flame, as it propagates in an $R = 10 L_f$ channel, is plotted for various conditions in Fig. 8. Here, Fig. 8a further confirms that the impact of the thermal expansion ratio on the flames is minor, especially if $Le \leq 1$. The impact of Θ on the flame is observed to increase at a higher Le , $Le = 2$. The maximum burning rates attained by the flame are observed to decrease with Θ at $Le \geq 1$. The reverse is however the case at $Le = 0.2$, as a crossover region exists between $Le = 0.2$ and $Le = 1$, where all thermal expansion ratios produce equal maximum burning rates. Considering a $\Theta = 8$ flame in the channels of various half-widths, Fig. 8b, we observe that the maximum burning rate increases with the channel widths for all the Lewis numbers investigated. The impact is however found to be more profound at high Le .

4b. Impact of thermal wall conditions

Flame propagation in channels with both extremes open and with nonslip and isothermal boundary conditions at the walls is also scrutinized – in order to identify the effect of thermal wall boundary conditions on the flame. The temperature snapshots shown in Fig. 9 is for the $\Theta = 8$ flame with various Lewis numbers in the range of $0.2 \leq Le \leq 2$, propagating in the channels of half-width $10 L_f$. When the channel wall is maintained at a temperature of $T_w = 300$ K, as shown in Fig. 9, a flame is qualitatively different from that seen in the adiabatic channels. Specifically, after an embryonic flame front is initiated using the ZFK planar approach, the flame front is observed to

retract, instead of propagating into the fuel premixtures, for all Le considered. Contraction of the flame is also observed to occur as heat is being lost to the channel wall. However, the rate at which such a flame retraction and contraction occurs changes with the Lewis number. For $Le = 0.2$ in Fig 9a, where mass diffusivity is dominant, both the retraction and contraction occur at a slower rate. The higher rate of mass diffusion into the flame front attempts to balance the heat being lost to the cold wall. When the mass diffusion balances or exceeds the thermal diffusion, we see the flame retracting and contracting slightly faster. The heat loss from the burnt gas to the cold wall, coupled with the distributed flow towards both exits, prevents the burnt gas from having the momentum required to push the fuel ahead of the flame front. Figures 9b and 9c present the flames with $Le = 1$ and 2, where the mass diffusion equals or exceeds the thermal diffusion, respectively. The rate of the flame retraction and contraction is shown to grow with Le .

The plots of the scaled flame tip position and the scaled burning rate for the flames with $\Theta = 8$ and various Lewis numbers, propagating in a channel of half-width $R = 10 L_f$ with isothermal wall, are shown in Fig. 10. Here, the evolution of the flame position also shows the flame retraction described earlier. Namely, the plot of the scaled flame tip position versus the scaled time, Fig. 10a, shows the flame tip moving towards the left open end of the channel, as opposed to travelling towards the right end, as was observed in semi-open channels as well as in adiabatic channels. The scaled burning rate versus the scaled time, Fig. 10b, also decreases for the $Le \geq 1$ flames. This was expected, since the flame morphology seen in the snapshots of Fig. 9 does not show any increase in the surface area of the flame front. For a wider channel, $R = 20 L_f$, the scaled flame tip position and the scaled burning rate are shown versus the scaled time in Figs. 11a and 11b, respectively. Again, we see the flame retreating, instead of advancing in Fig. 11a. However, the retraction here happened at a slower rate.

Also, a deviation from the generally observed flame behavior is obtained for a low Lewis number, $Le = 0.2$, as such a flame is seen to have changed direction at a point in the channel. The scaled flame tip thereafter shows an upward trend, Fig. 11a. The same trend is revealed in the plot of the scaled burning rate shown in Fig. 11b. Such a slight change in the flame behavior when the channel half-width is increased from $10 L_f$ to $20 L_f$ can be attributed to the impact of heat loss to the channel wall. While both channels have their walls kept at 300 K, the impact of the heat loss is more significant in a narrower channel. The reason being that, the narrower the channel is, the higher the surface to volume ratio is and, consequently, the higher the impact of the heat loss is.

Overall, we may conclude that the role of the thermal boundary conditions at the channel walls is important and may potentially dominate over that of the Lewis number (although the impact of the isothermal walls, cold and preheated, needs to be further investigated elsewhere). At the same time, the impact of Le on burning in the isothermal $T_w = 300$ K channels is qualitatively weaker than that in the adiabatic channels.

5. Conclusions

In this work, we have studied the impact of the Lewis number, Le , on propagation of the premixed flames in channels with both ends open, and with smooth, nonslip walls – either adiabatic or isothermal. Also, scrutinized is an interplay of nonequidiffusive burning with thermal expansion and the channel geometry. The analysis is performed by means of numerical simulations of the reacting flow equations, with fully compressible hydrodynamics and one-step Arrhenius chemical kinetics. We started with the adiabatic wall condition as the main case of study in this work. It is found that the flames oscillate at low Lewis numbers, $Le < 1$, with the oscillation amplitude and frequency decreasing with Le . The low- Le flames exhibit the stages of cusp formation, flame bifurcation and the collapse of the flame segments, repeatedly. For the $Le \geq 1$ flames, slight

oscillations are seen right after initiation, followed by steady flame propagation. While the effect of the thermal expansion ratio on the flame dynamics and morphology is found to be minimal, the trend of its impact at $Le = 0.2$ is reversed when $Le = 2$. An increase in the channel width produces a slight difference in the flame behavior, while the differences in morphology and dynamics are much more notable at $Le = 0.2$. While the majority of the simulation runs of the present work employed the adiabatic wall condition, for comparison, the analysis was subsequently extended to the isothermal channels. It is shown that the role of heat losses to the walls is important and may potentially dominate over that of the Lewis number. At the same time, the impact of Le on burning in the isothermal channels is qualitatively weaker than that in the adiabatic channels.

Acknowledgements

This study at West Virginia University was sponsored by the U.S. National Science Foundation (NSF) through the CAREER Award #1554254 (V.A.) as well as by the West Virginia Higher Education Policy Commission through the grant #HEPC.dsr.18.7 (V.A.). D. V. was supported by the National Science Foundation of China (NSFC) through the grant number 51750110503.

Data Availability Statement

The data that support the findings of this study are available from the corresponding author upon reasonable request.

References

- [1] C.K. Law, *Combustion Physics*. New York: Cambridge University Press, 2006.
- [2] M. Hasanuzzaman, M.M. Rahman, H.F. Öztop, N.A. Rahim, R. Saidur, "Effects of Lewis number on heat and mass transfer in a triangular cavity," *Int. Commun. Heat Mass Transf.*, vol. 39, no. 8, pp. 1213–1219, 2012.
- [3] C. Dopazo, L. Cifuentes, N. Chakraborty, "Vorticity budgets in premixed combustng turbulent flows at different Lewis numbers," *Phys. Fluids*, vol. 29, no. 4, p. 045106, 2017.
- [4] S. Kadowaki, T. Hasegawa, "Numerical simulation of dynamics of premixed flames: flame instability and vortex-flame interaction," *Prog. En. Combust. Sci.*, vol. 31, pp. 193-241, 2005.
- [5] N. Chakraborty, I. Konstantinou, A. Lipatnikov, "Effects of Lewis number on vorticity and enstrophy transport in turbulent premixed flames," *Phys. Fluids*, vol. 28, no. 1, p. 015109, 2016.
- [6] N. Chakraborty, R. Cant, "Effects of Lewis number on turbulent scalar transport and its modelling in turbulent premixed flames," *Combust. Flame*, vol. 156, no. 7, pp. 1427–1444, 2009.
- [7] N. Chakraborty, R.S. Cant, "Effects of Lewis number on flame surface density transport in turbulent premixed combustion," *Combust. Flame*, vol. 158, no. 9, pp. 1768–1787, 2011.
- [8] Y. Ju, H. Guo, F. Liu, K. Maruta, "Effects of the Lewis number and radiative heat loss on the bifurcation and extinction of CH₄/O₂-N₂-He flames," *J. Fluid Mech.*, vol. 379, pp. 165–190, 1999.
- [9] S.D. Salusbury, J.M. Bergthorson, "Maximum stretched flame speeds of laminar premixed counter-flow flames at variable Lewis number," *Combust. Flame*, vol. 162, no. 9, pp. 3324–3332, 2015.
- [10] S.H. Yoon, T.J. Noh, O. Fujita, "Effects of Lewis number on generation of primary acoustic instability in downward-propagating flames," *Proc. Combust. Inst.*, vol. 36, no. 1, pp. 1603–1611, 2017.
- [11] J.B. Bell, R.K. Cheng, M.S. Day, I.G. Shepherd, "Numerical simulation of Lewis number effects on lean premixed turbulent flames," *Proc. Combust. Inst.* vol. 31, p. 1309, 2007.
- [12] L. Berger, K. Kleinheinz, A. Attili, H. Pitsch, "Characteristic patterns of thermodiffusively unstable premixed lean hydrogen flames," *Proc. Combust. Inst.* vol. 37, pp. 1879-1886, 2019.
- [13] V.N. Kurdyumov, "Lewis number effect on the propagation of premixed flames in narrow adiabatic channels : Symmetric and non-symmetric flames and their linear stability analysis," *Combust. Flame*, vol. 158, no. 7, pp. 1307–1317, 2011.
- [14] M. Alkhabbaz, O. Abidakun, D. Valiev, V. Akkerman, "Impact of the Lewis number on flame acceleration at the early stage of burning in pipes," *Phys. Fluids*, vol. 31, no. 8, 083606, 2019.
- [15] M. Sánchez-Sanz, D. Fernández-Galisteo, V.N. Kurdyumov, "Effect of the equivalence ratio, Damköhler number, Lewis number and heat release on the stability of laminar premixed flames in microchannels," *Combust. Flame*, vol. 161, no. 5, pp. 1282–1293, 2014.
- [16] S. Chakraborty, A. Mukhopadhyay, S. Sen, "Interaction of Lewis number and heat loss effects for a laminar premixed flame propagating in a channel," *Int. J. Therm. Sci.*, vol. 47, no. 1, pp. 84–92, 2008.

- [17] A. Adebisi, O. Abidakun, G. Idowu, D. Valiev, V. Akkerman, "Analysis of nonequidiffusive premixed flames in obstructed channels," *Phys. Rev. Fluids*, vol. 4, no. 6, p. 063201, 2019.
- [18] A. Petchenko, V. Bychkov, V. Akkerman, L.-E. Eriksson, "Flame-sound interaction in tubes with nonslip walls," *Combust. Flame*, vol. 149, no. 4, pp. 418–434, 2007.
- [19] A. Petchenko, V. Bychkov, V. Akkerman, L.-E. Eriksson, "Violent folding of a flame front in a flame-acoustic resonance," *Phys. Rev. Lett.* vol. 97, no. 16, 164501 2006.
- [20] F. Veiga-López, D. Martínez-Ruiz, E. Fernández-Tarrazo, M. Sánchez-Sanz, "Experimental analysis of oscillatory premixed flames in a Hele-Shaw cell propagating towards a closed end," *Combust. Flame*, vol. 201, pp. 1–11, 2019.
- [21] V. Akkerman, V. Bychkov, A. Petchenko, L.-E. Eriksson, "Flame oscillations in tubes with nonslip at the walls," *Combust. Flame*, vol. 145, no. 4, pp. 675–687, 2006.
- [22] C. Cui, M. Matalon, T.L. Jackson, "Pulsating mode of flame propagation in two-dimensional channels," *AIAA Journal*, vol. 43, p. 1284, 2005.
- [23] G. Pizza, C.E. Frouzakis, J. Mantzaras, A.G. Tomboulides, K. Boulouchos, "Dynamics of premixed hydrogen/air flames in microchannels," *Combust. Flame*, vol. 152, no. 3, pp. 433–450, 2008.
- [24] N. Andersson, L.-E. Eriksson, L. Davidson, "Large-eddy simulation of subsonic turbulent jets and their radiated sound," *AIAA Journal*, vol. 43, no. 9, pp. 1899–1912, 2005.
- [25] V.V. Bychkov, S.M. Golberg, M.A. Liberman, L.-E. Eriksson, "Propagation of curved stationary flames in tubes," *Phys. Rev. E*, vol. 54, no. 4, pp. 3713–3724, 1996.
- [26] M. Liberman, M. Ivanov, O. Peil, D. Valiev, L.-E. Eriksson, "Numerical studies of curved stationary flames in wide tubes," *Combust. Theory Modell.* vol. 7, no. 4, pp. 653–676, 2003.
- [27] D. Valiev, V. Bychkov, V. Akkerman, L.-E. Eriksson, C.K. Law, "Quasi-steady stages in the process of premixed flame acceleration in narrow channels," *Phys. Fluids*, vol. 25, no. 9, p. 096101, 2013.
- [28] A. Adebisi, E. Ridgeway, R. Alkandari, A. Cathreno, D. Valiev, V. Akkerman, "Premixed flame oscillations in obstructed channels with both ends open," *Proc. Combust. Inst.*, vol. 37, no. 2, pp. 1919–1926, 2019.
- [29] G. Ciccarelli, S. Dorofeev, "Flame acceleration and transition to detonations in ducts," *Prog. Energy Combust. Sci.*, vol. 34, pp. 499–550, 2008.

FIGURES

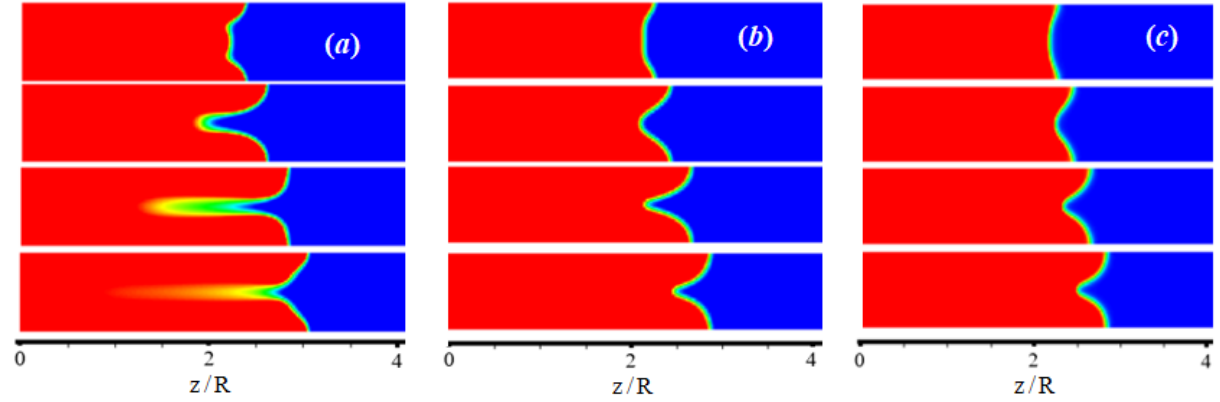


Figure 1: The color temperature snapshots, from $T = 300$ K in the fuel mixture (blue) till $T = 1500$ K in the burnt matter (red), for the evolution of the $\Theta = 5$ flames with various Lewis numbers: $Le = 0.2$ (a), $Le = 1$ (b) and $Le = 2$ (c) propagating in the adiabatic channel of half-width $R = 10 L_f$ in all three cases.

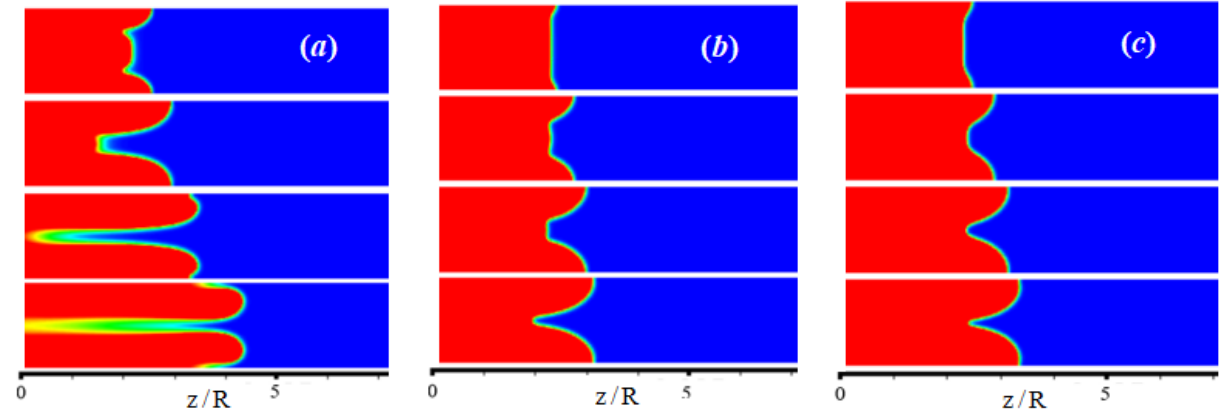


Figure 2: The color temperature snapshots, from $T = 300$ K in the fuel mixture (blue) till $T = 1500$ K in the burnt matter (red), for the evolution of the $\Theta = 5$ flames with various Lewis numbers: $Le = 0.2$ (a), $Le = 1$ (b) and $Le = 2$ (c) propagating in the adiabatic channel of half-width $R = 20 L_f$ in all three cases.

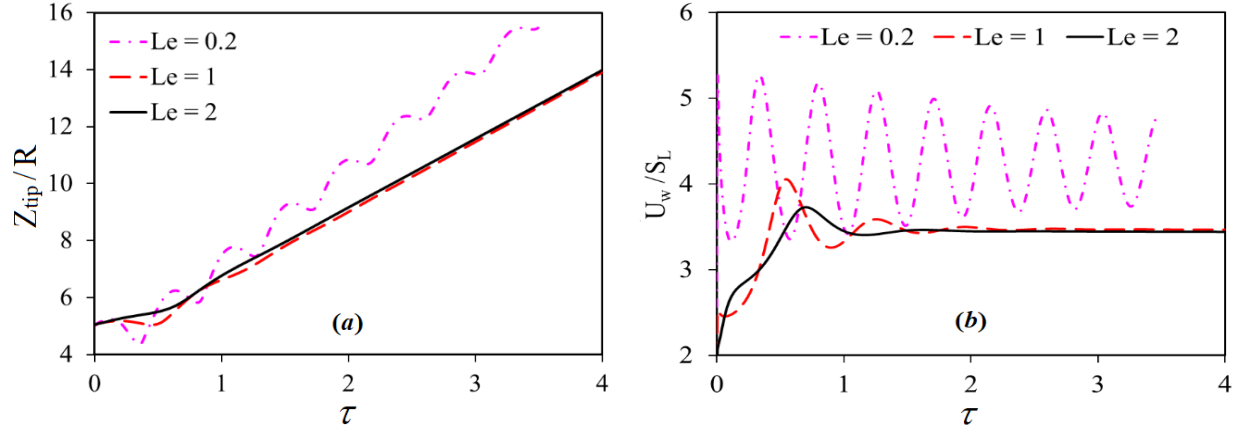


Figure 3: The scaled flame tip positions Z_{tip}/R (a) and the scaled burning rate U_w/S_L (b) versus scaled time $\tau = tS_L/R$ for the $\Theta = 5$ flames with various $Le = 0.2, 1$, and 2 propagating in the adiabatic channel of half-width $R = 10 L_f$.

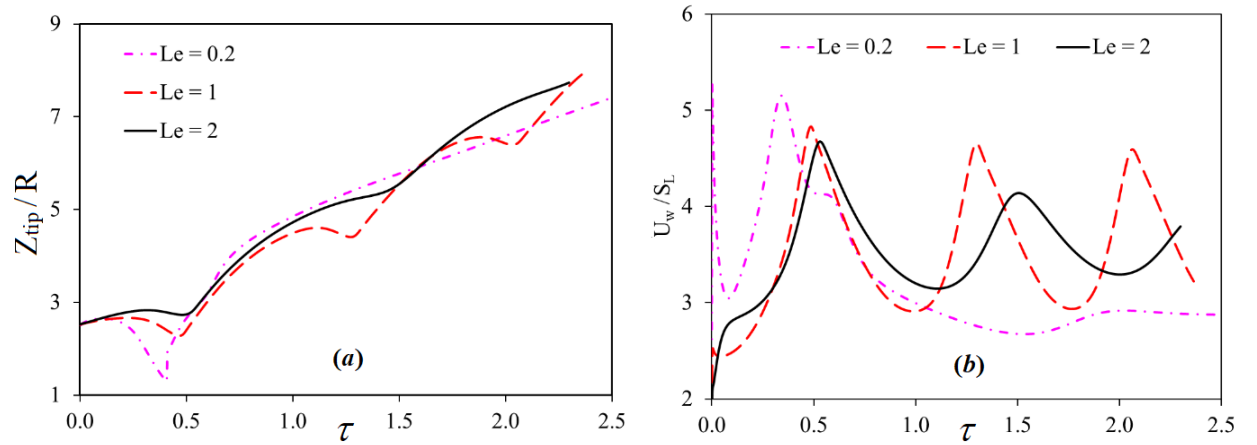


Figure 4: The scaled flame tip positions Z_{tip}/R (a) and the scaled burning rate U_w/S_L (b) versus scaled time $\tau = tS_L/R$ for the $\Theta = 5$ flames with various $Le = 0.2, 1$ and 2 propagating in the adiabatic channel of half-width $R = 20 L_f$.

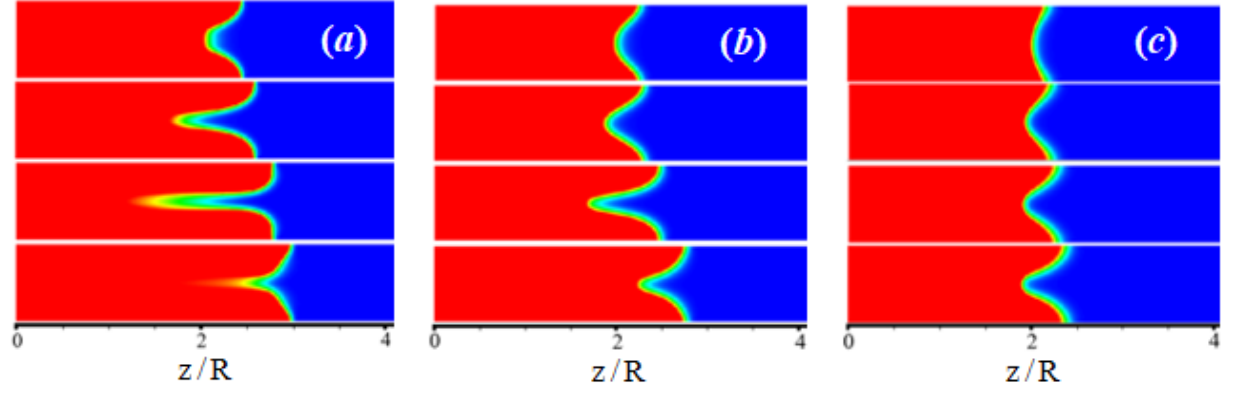


Figure 5: The color temperature snapshots, from $T = 300$ K in the fuel mixture (blue) till $T = 3000$ K in the burnt gas (red), for the evolution of the $\Theta = 10$ flames in the channels with $R = 20 L_f$, $Le = 0.2$ (a) $R = 10 L_f$, $Le = 0.2$ (b); and $R = 10 L_f$, $Le = 2$ (c).

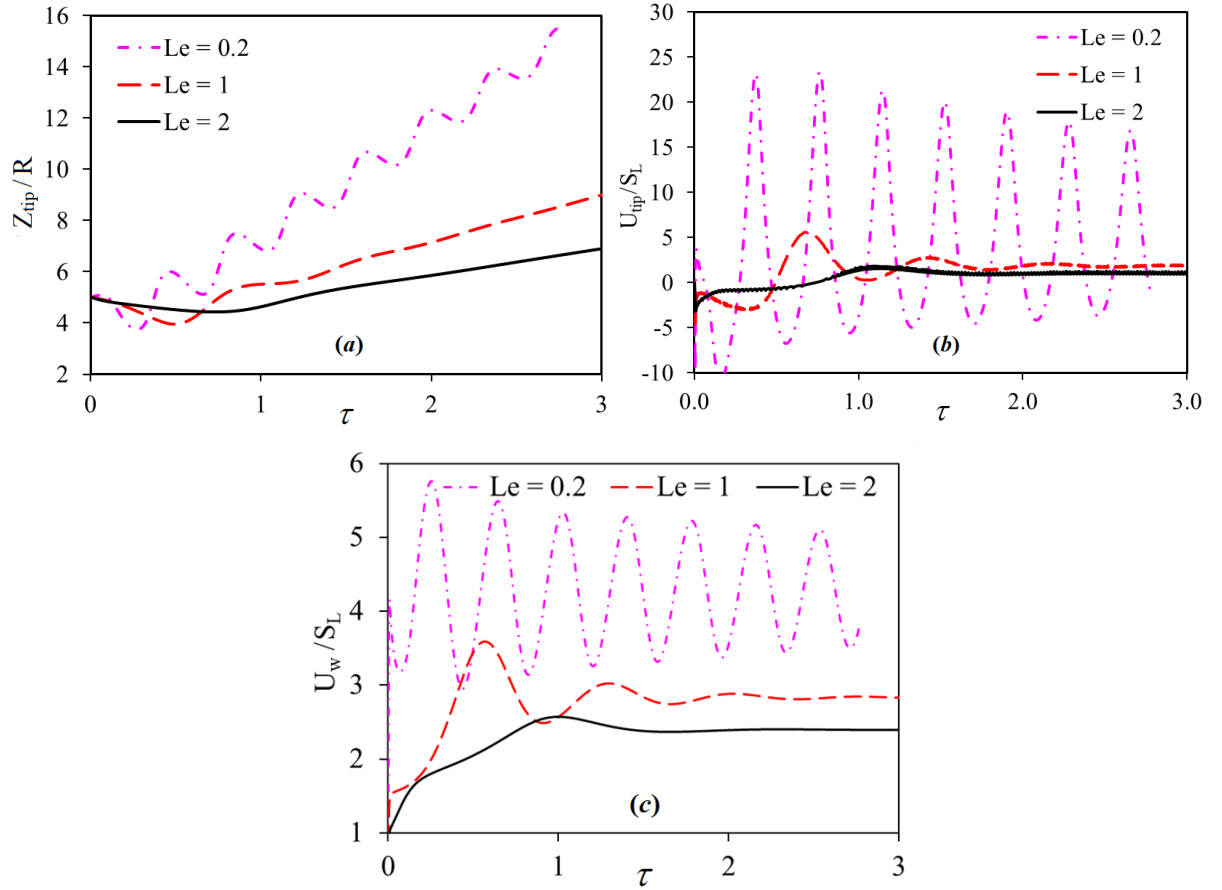


Figure 6: The scaled flame tip positions Z_{tip}/R (a), the scaled flame tip velocity U_{tip}/R (b) and the scaled burning rate U_w/S_L (c) versus scaled time $\tau = tS_L/R$ for the $\Theta = 10$ flames with various $Le = 0.2, 1$ and 2 propagating in the adiabatic channel of half-width $R = 10 L_f$.

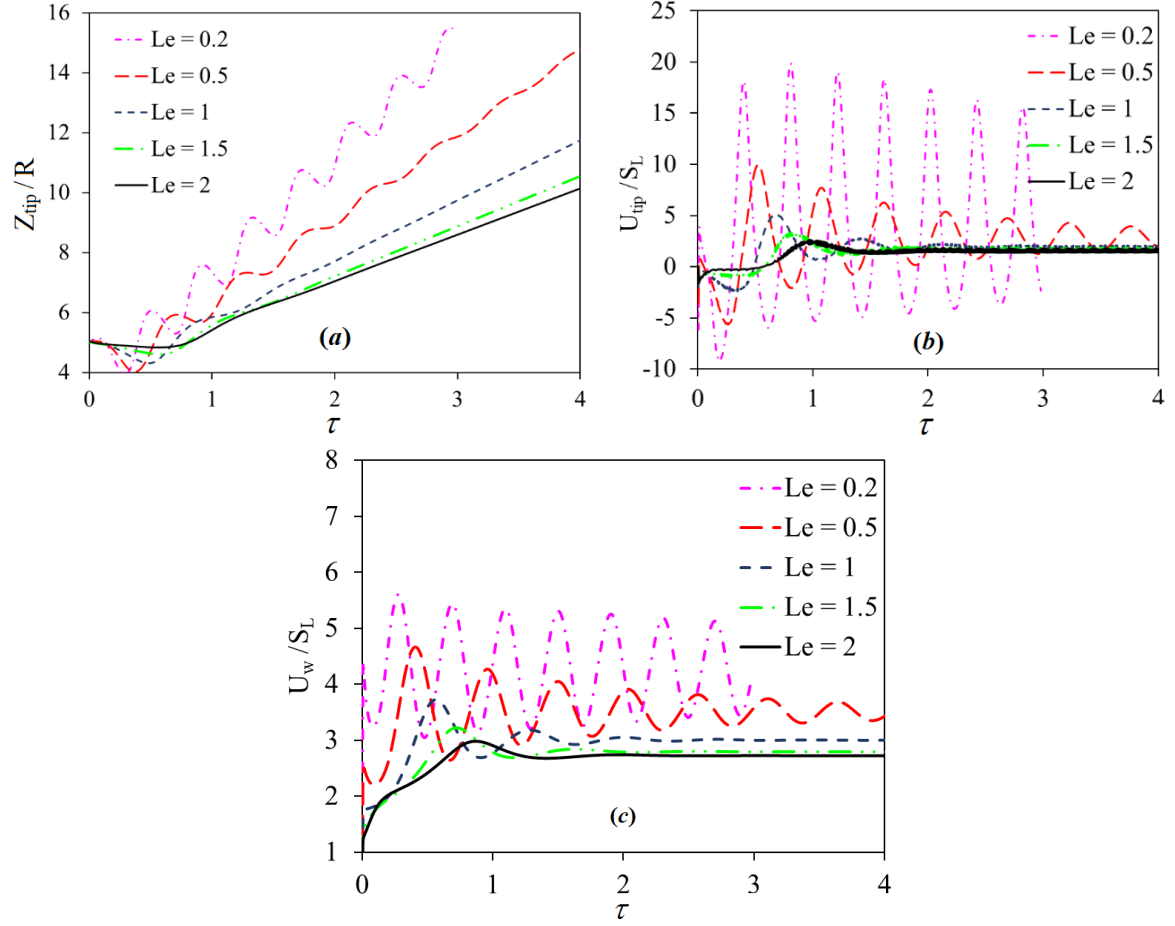


Figure 7: The scaled flame tip positions Z_{tip}/R (a), the scaled flame tip velocity U_{tip}/R (b) and the scaled burning rate U_w/S_L (c) versus scaled time $\tau = tS_L/R$ for the $\Theta = 8$ flames with various $Le = 0.2, 0.5, 1, 1.5$ and 2 propagating in the adiabatic channel of half-width $R = 10 L_f$.

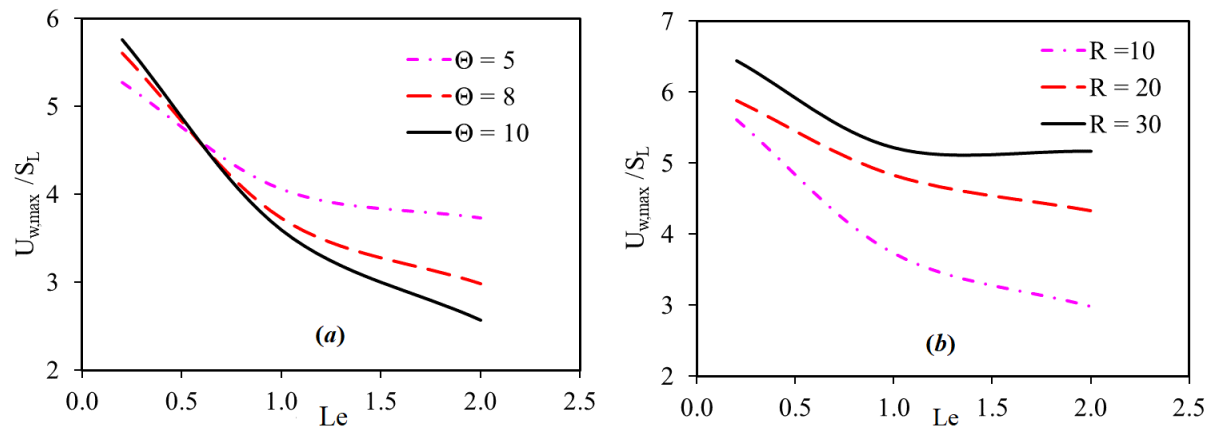


Figure 8: The scaled maximum burning rate $U_{w,max}/S_L$ versus the Lewis number Le for (a) flames of various expansion ratios $\Theta = 5, 8, 10$, propagating in the adiabatic channel of half-width $R = 10 L_f$, and (b) flames with $\Theta = 8$, propagating in the adiabatic channels of scaled half-widths $R/L_f = 10, 20, 30$.

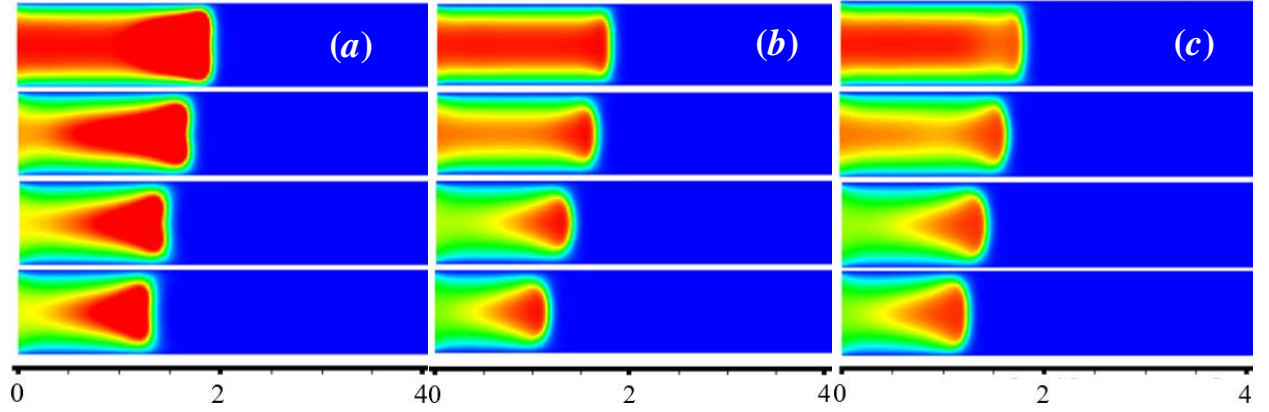


Figure 9: The temperature snapshots, from $T = 300$ K in the fuel mixture (blue) till $T = 2400$ K in the burnt matter (red), for the evolutions of the $\Theta = 8$ flames with various $Le = 0.2$ (a), $Le = 1$ (b), and $Le = 2$ (c) propagating in the isothermal ($T_w = 300$ K) channel of $R = 10 L_f$.

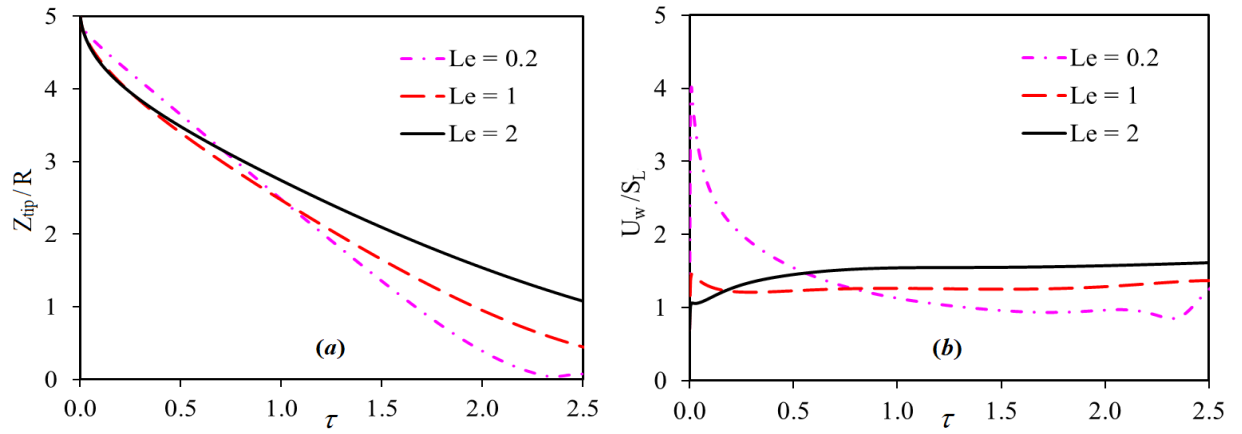


Figure 10: The scaled flame tip positions Z_{tip}/R (a) and the scaled burning rate U_w/S_L (b) versus the scaled time $\tau = tS_L/R$ for the $\Theta = 8$ flames with various $Le = 0.2, 1$ and 2 propagating in the isothermal ($T_w = 300$ K) channel of $R = 10 L_f$.

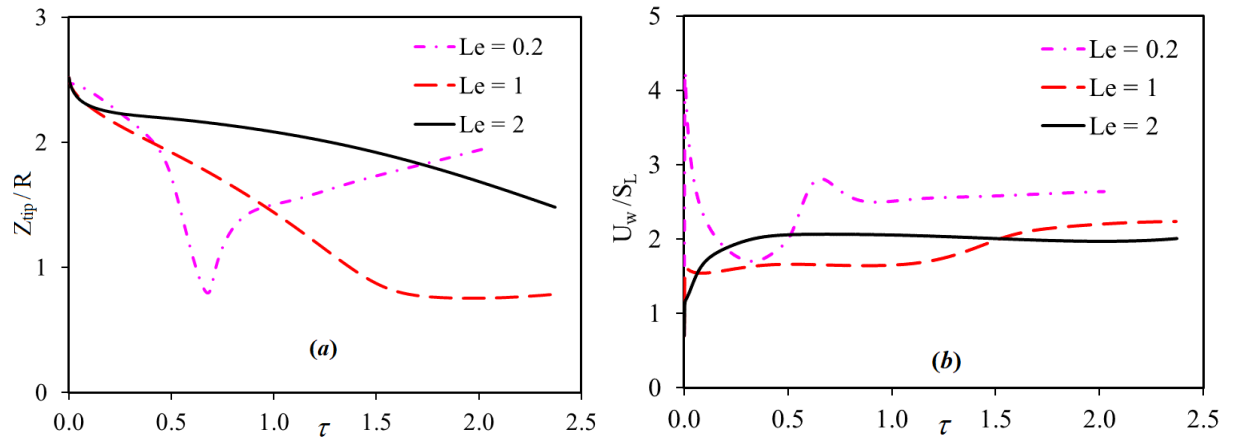
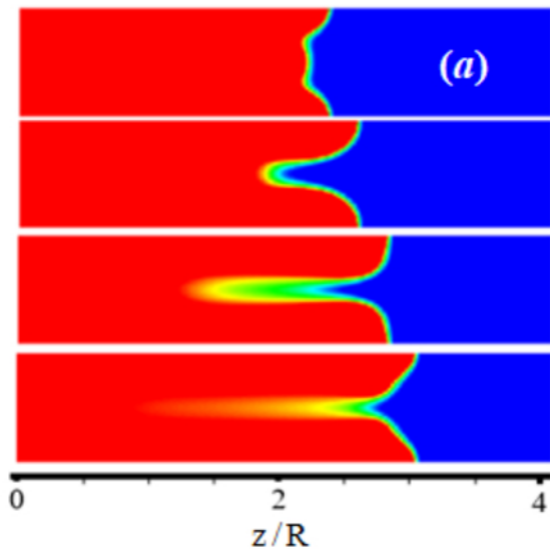
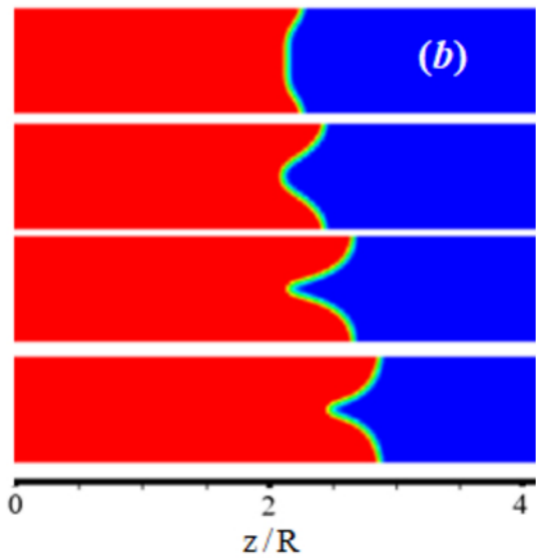
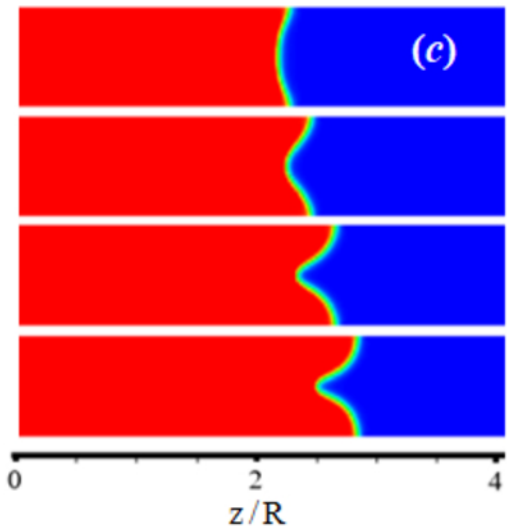
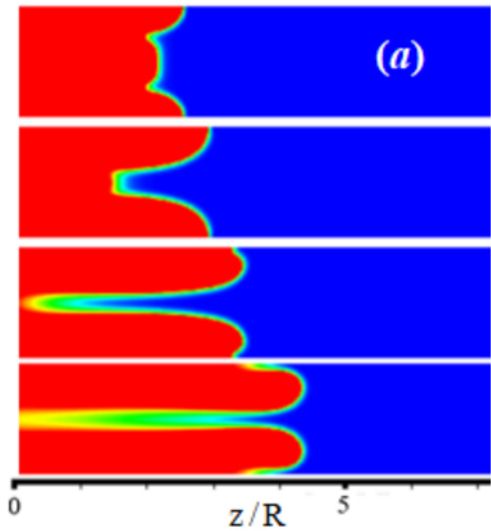


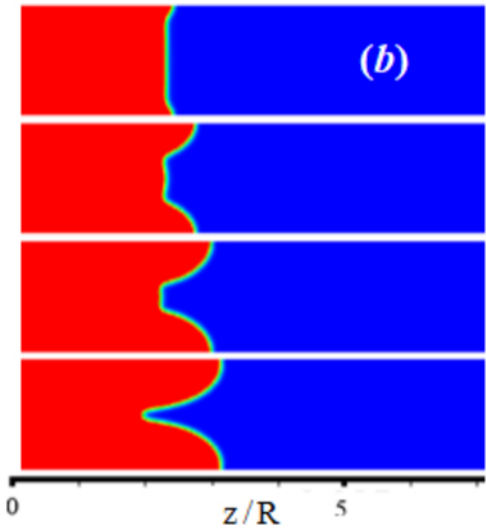
Figure 11: The scaled flame tip positions Z_{tip}/R (a) and the scaled burning rate U_w/S_L (b) versus scaled time $\tau = tS_L/R$ for the $\Theta = 8$ flames with various $Le = 0.2, 1$ and 2 propagating in the isothermal ($T_w = 300$ K) channel of $R = 20 L_f$.

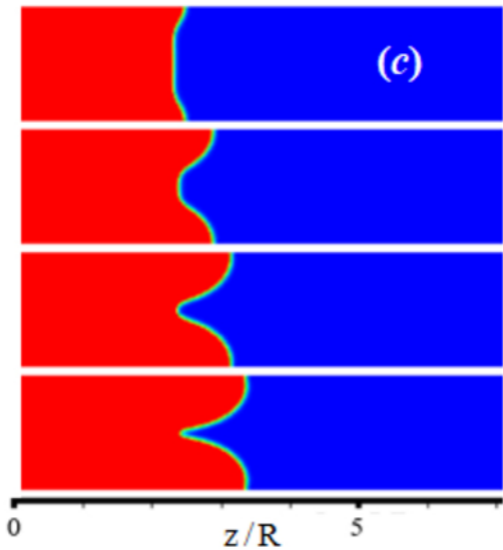


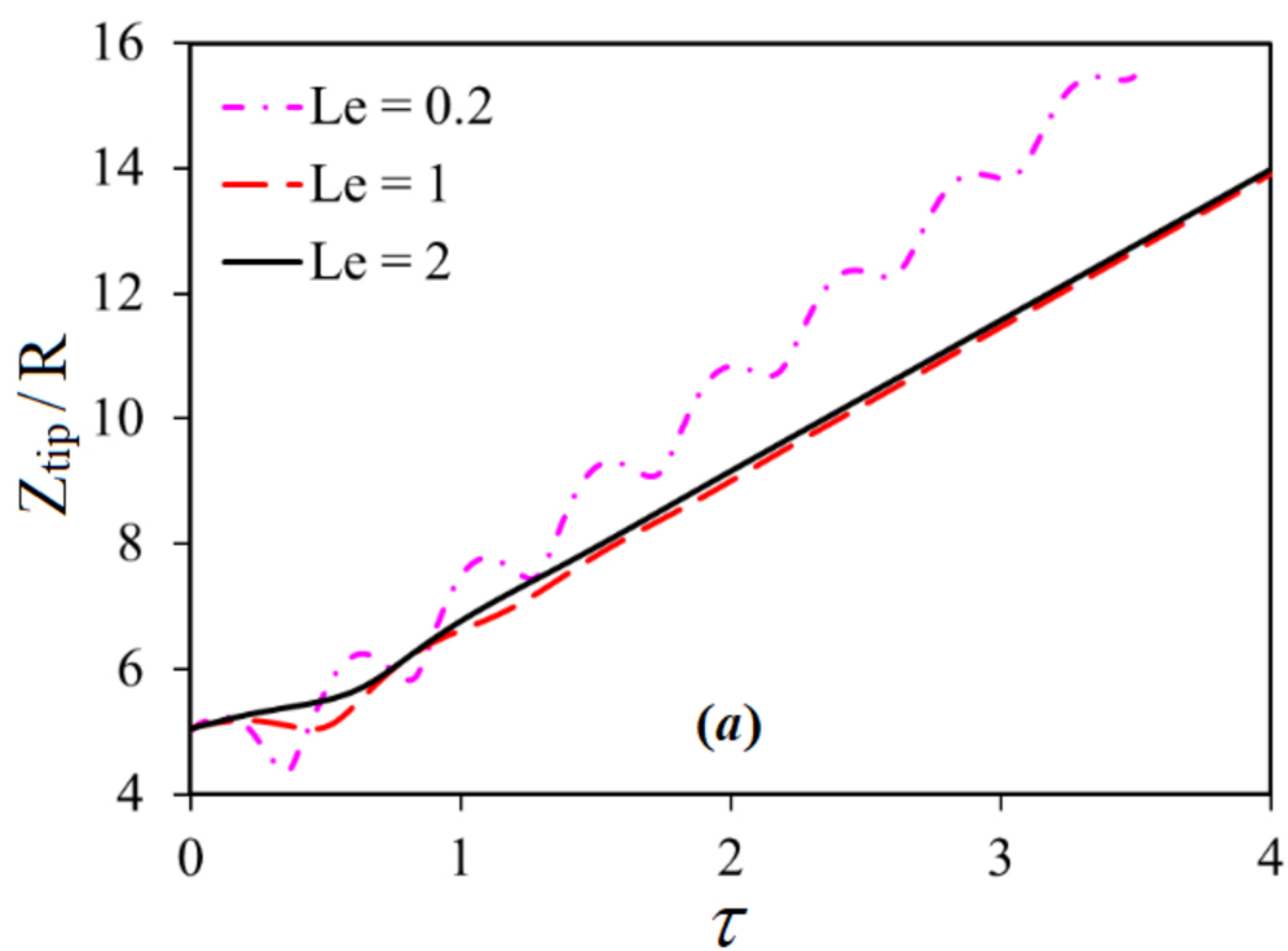


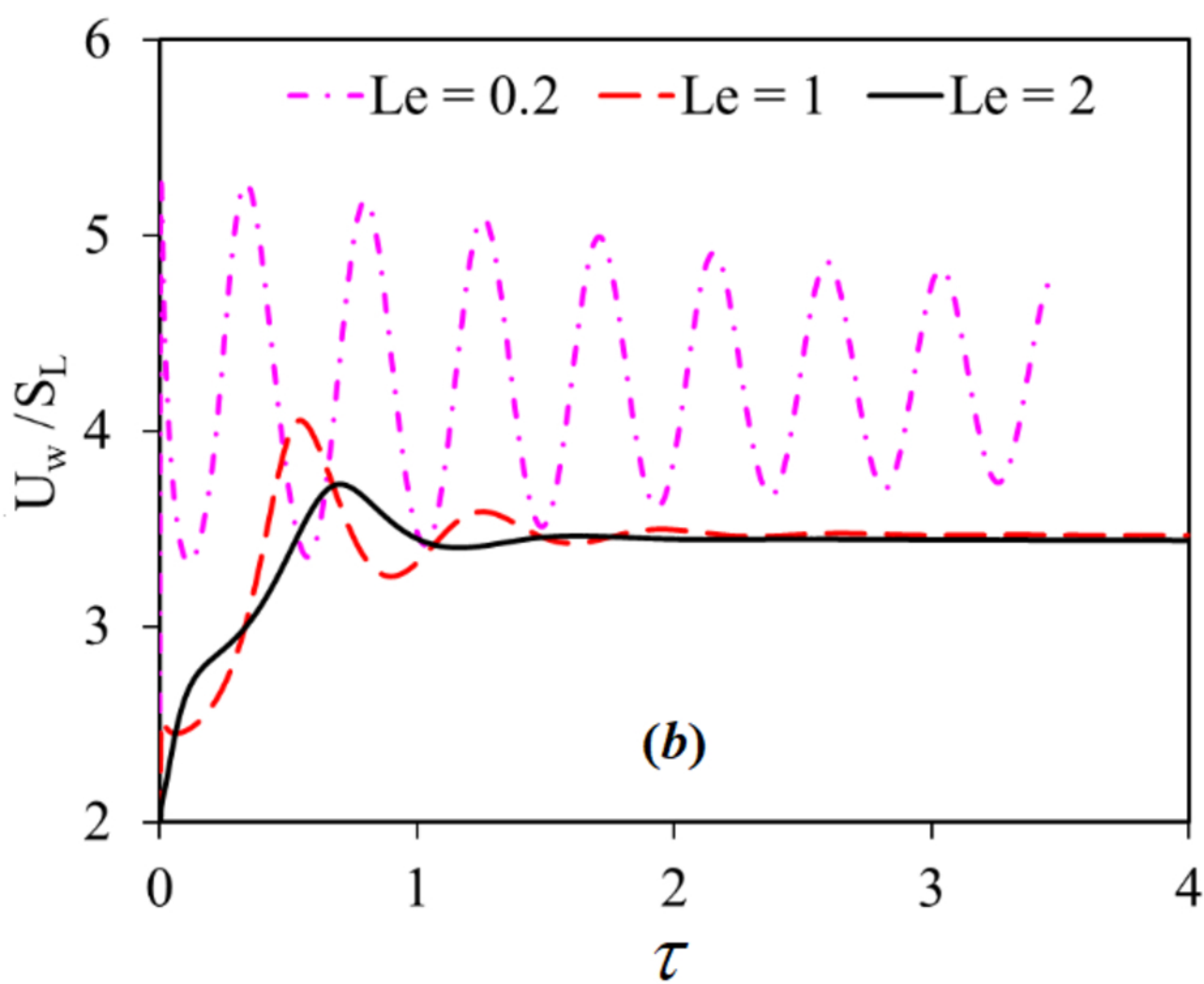


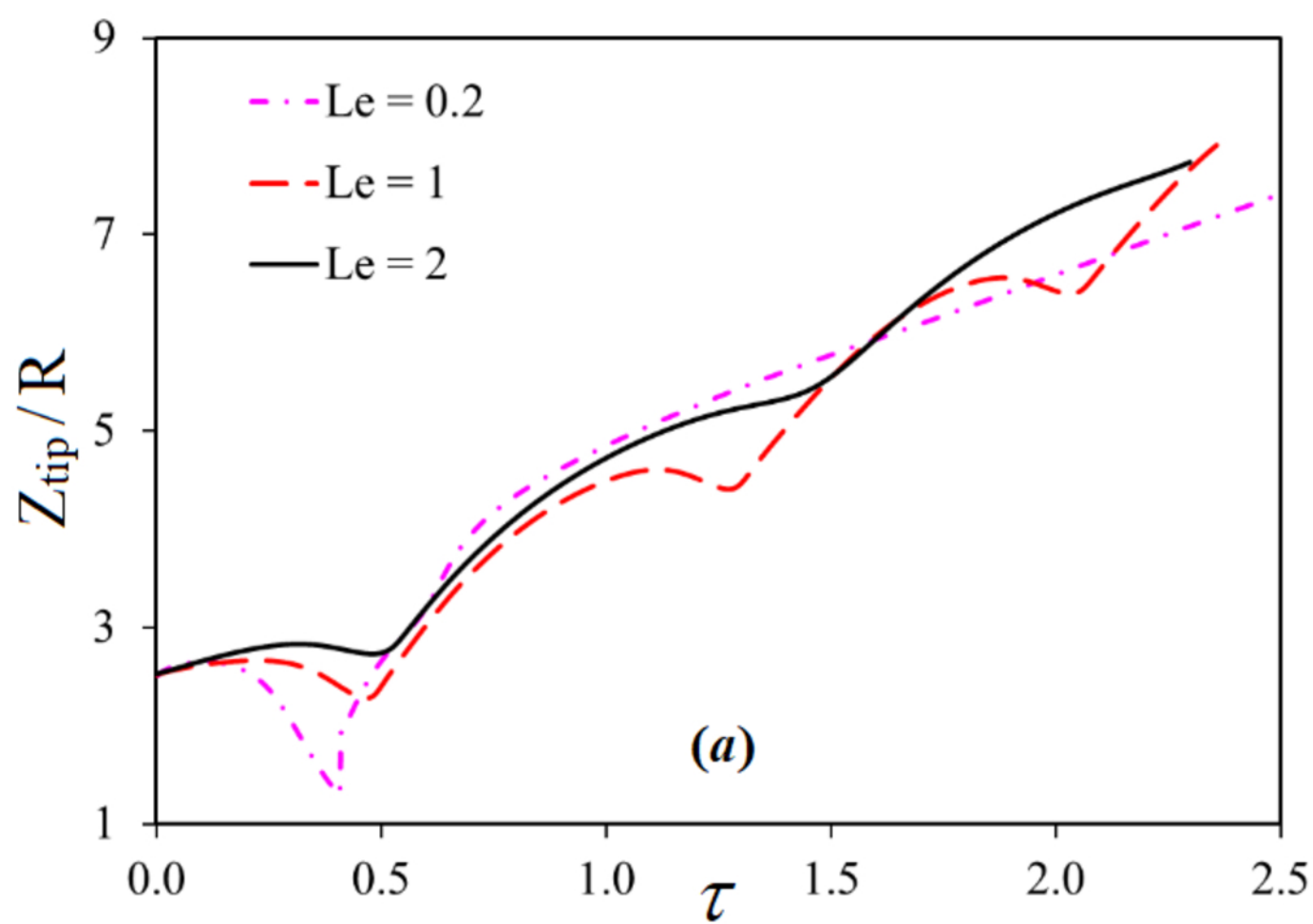


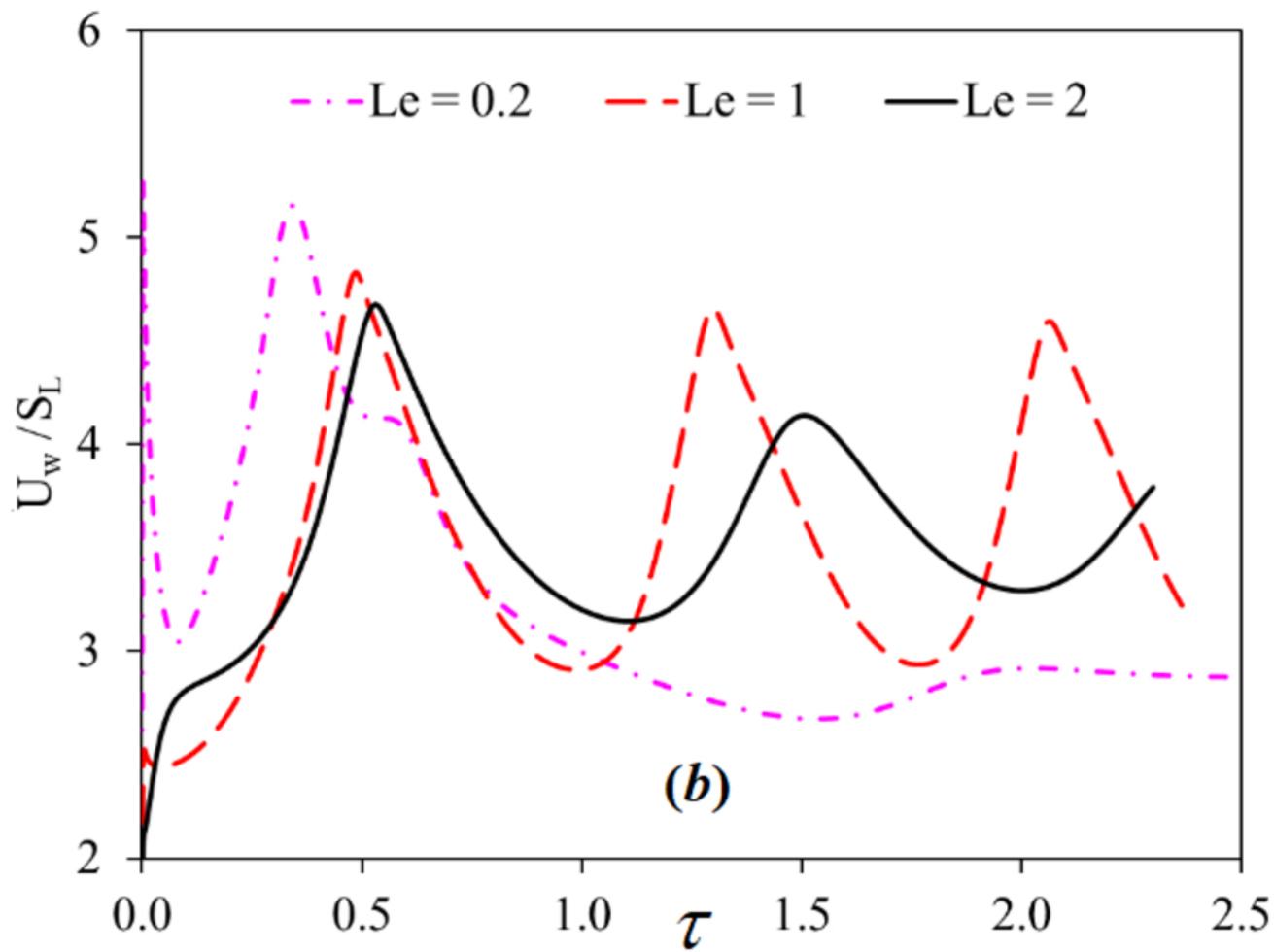


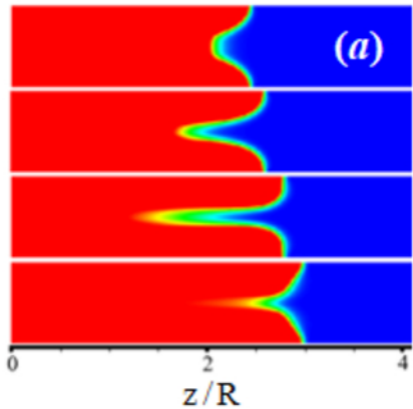


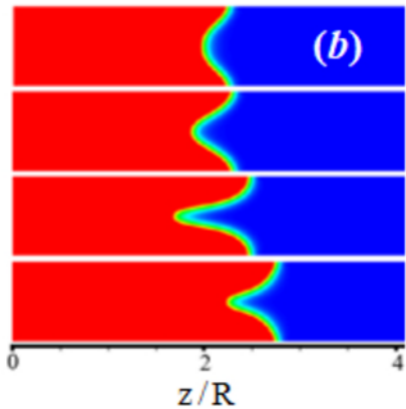


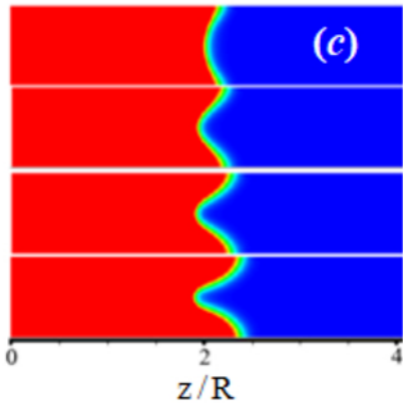


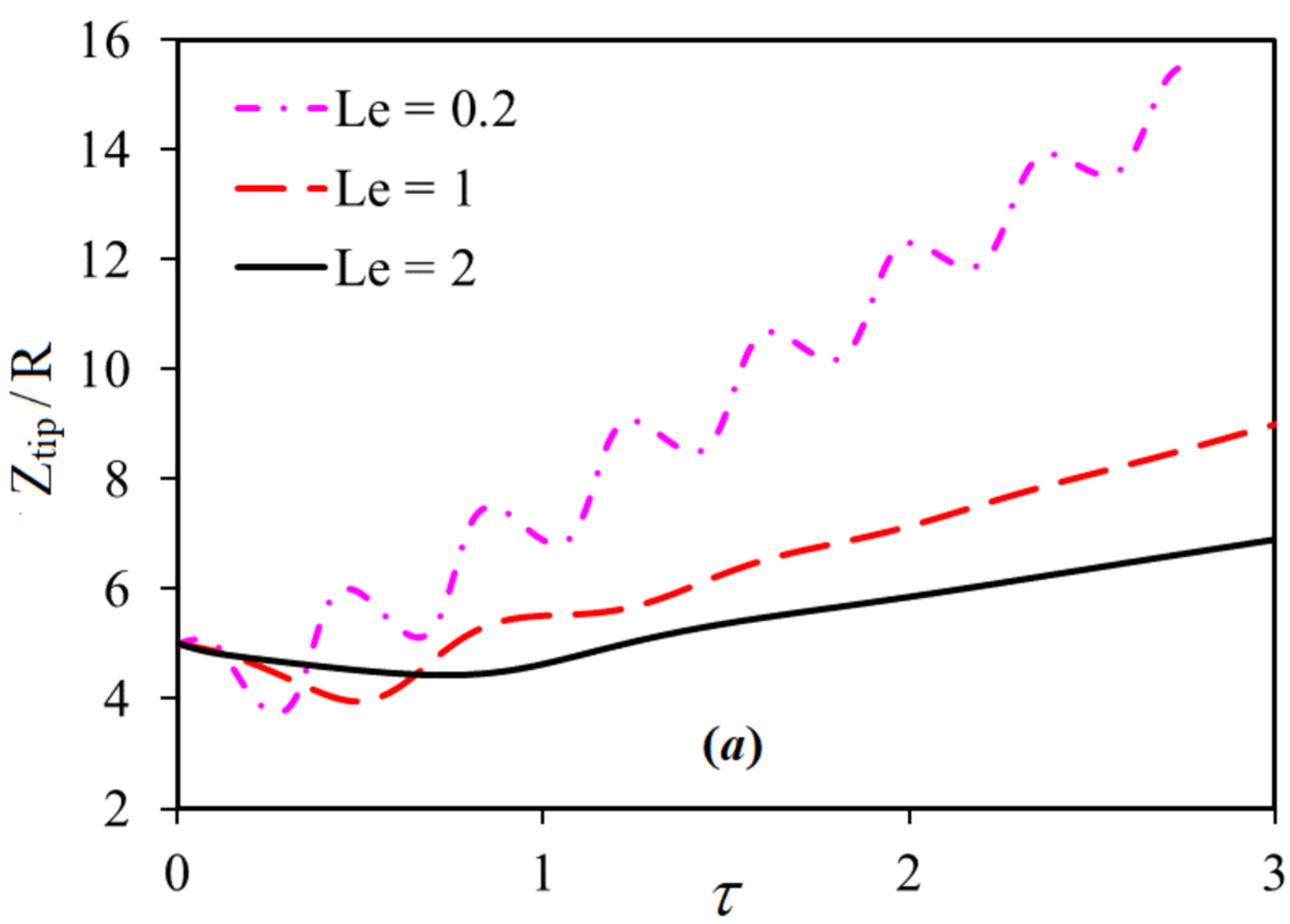


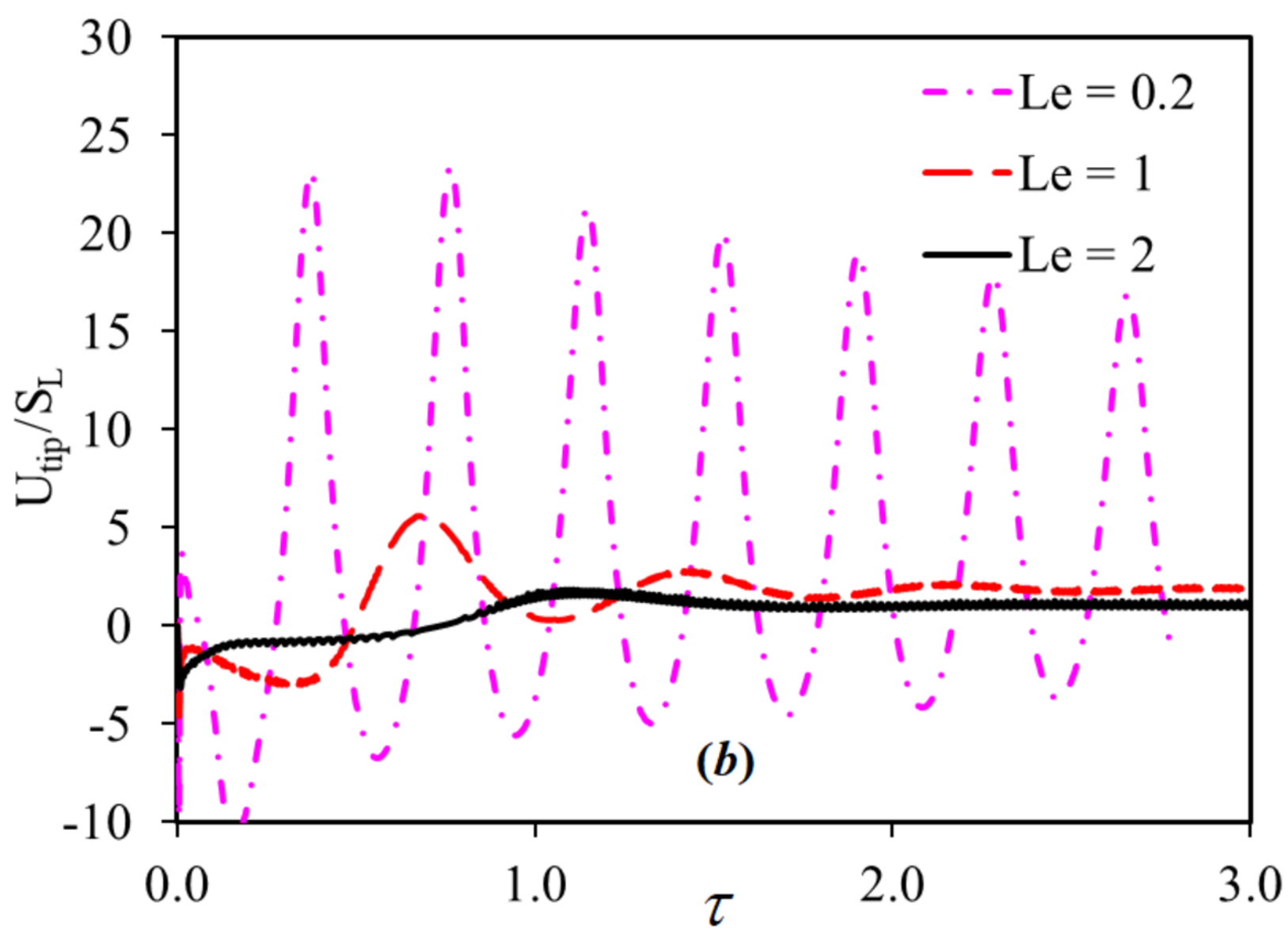


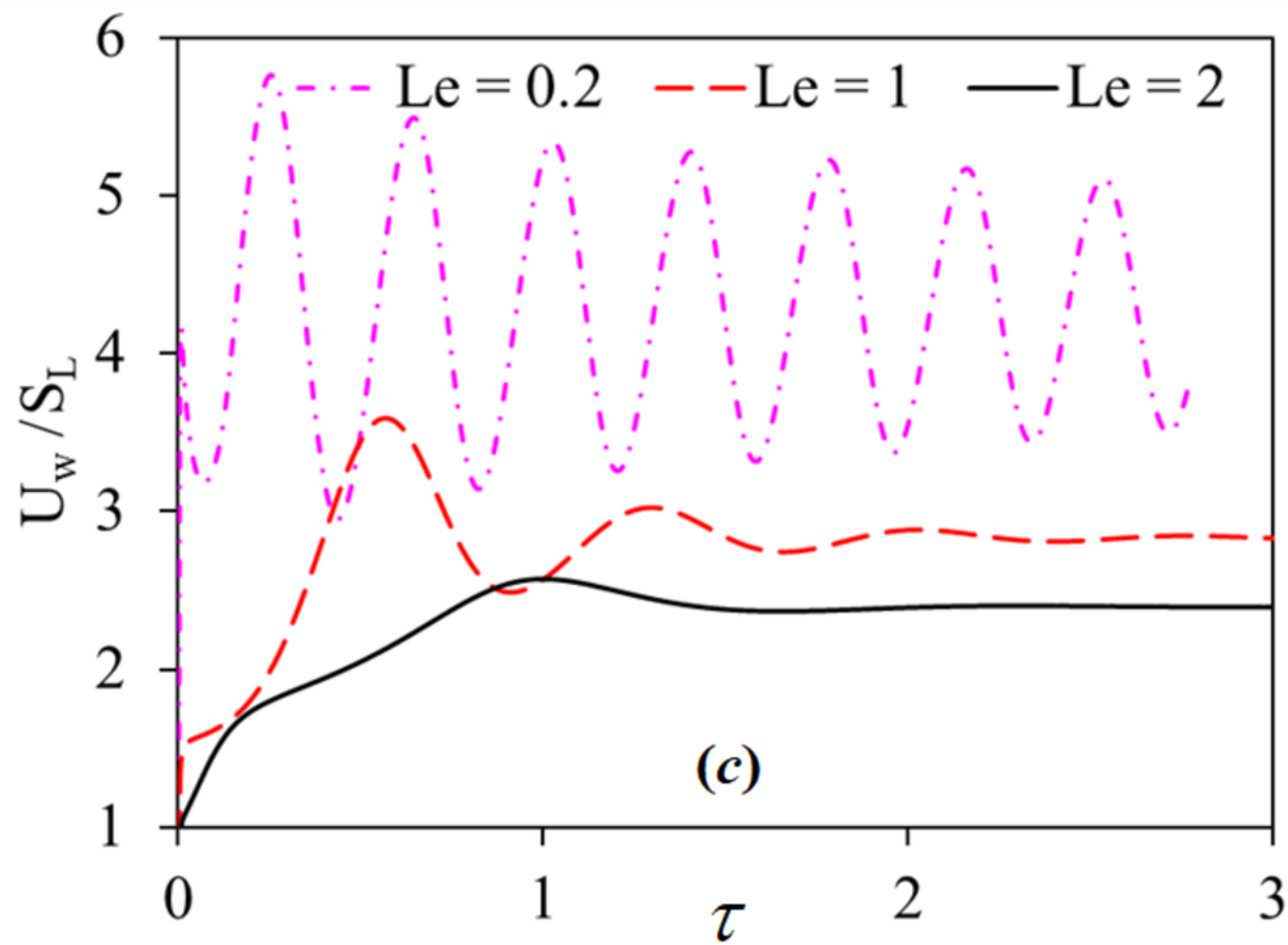


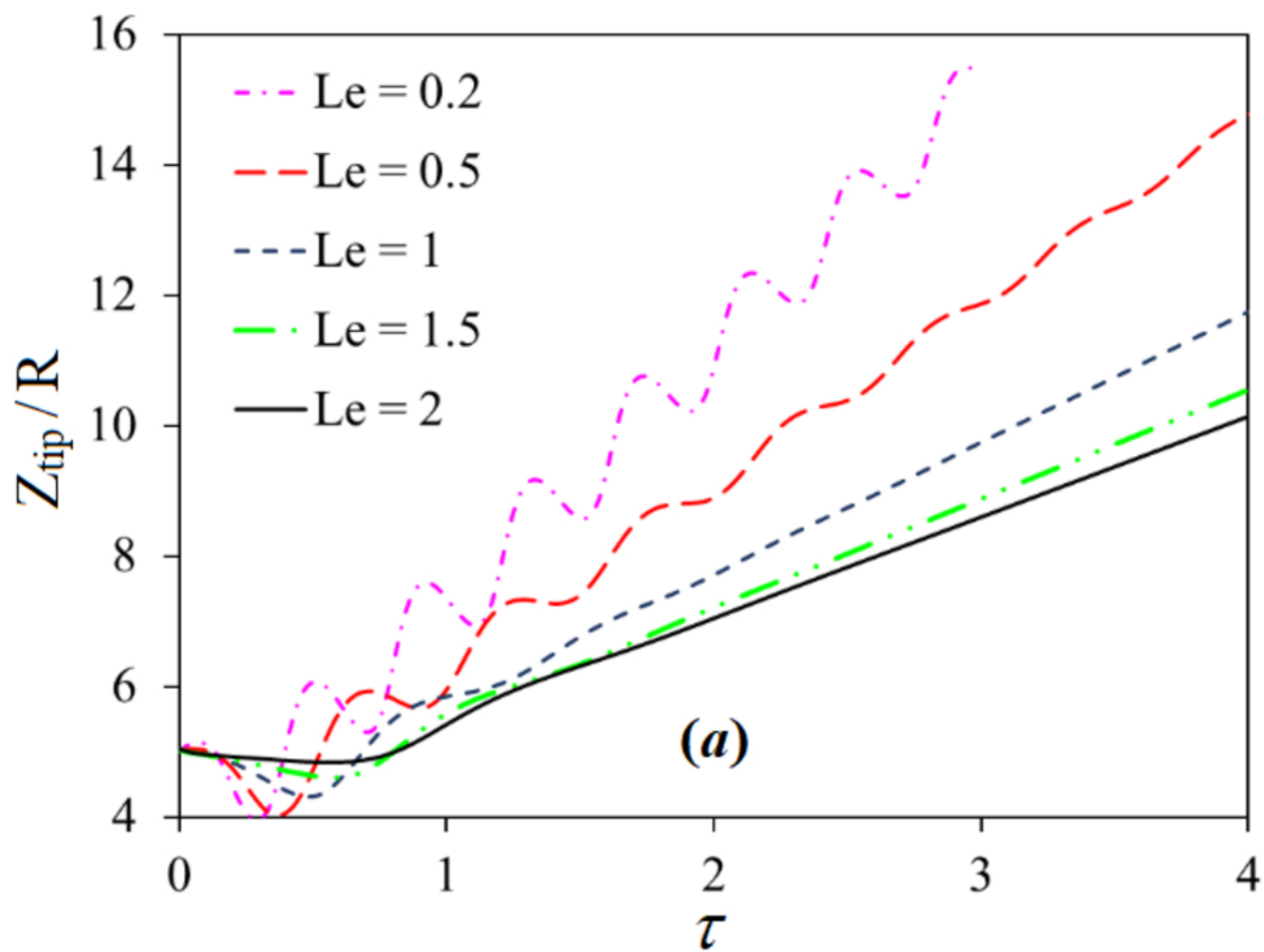


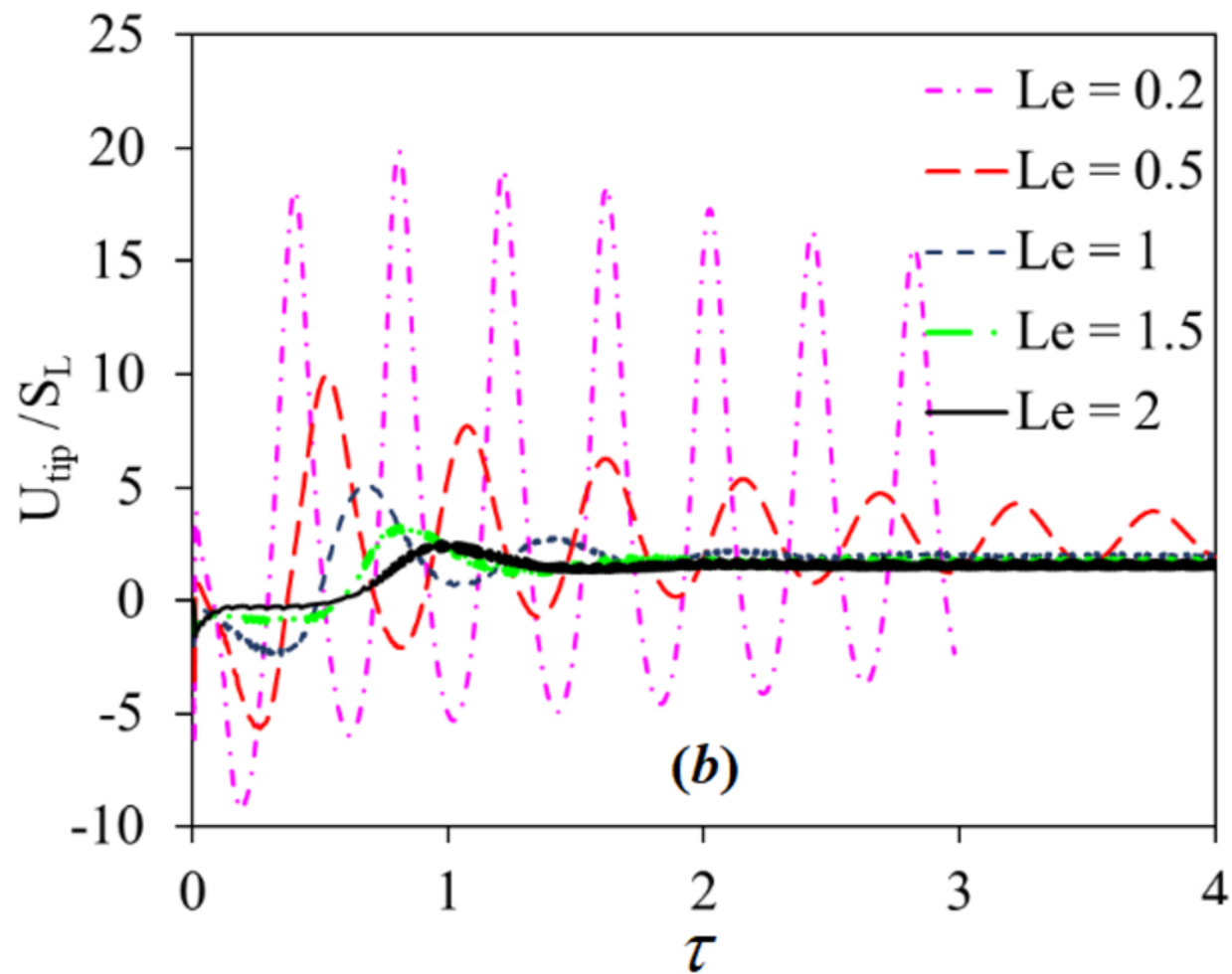


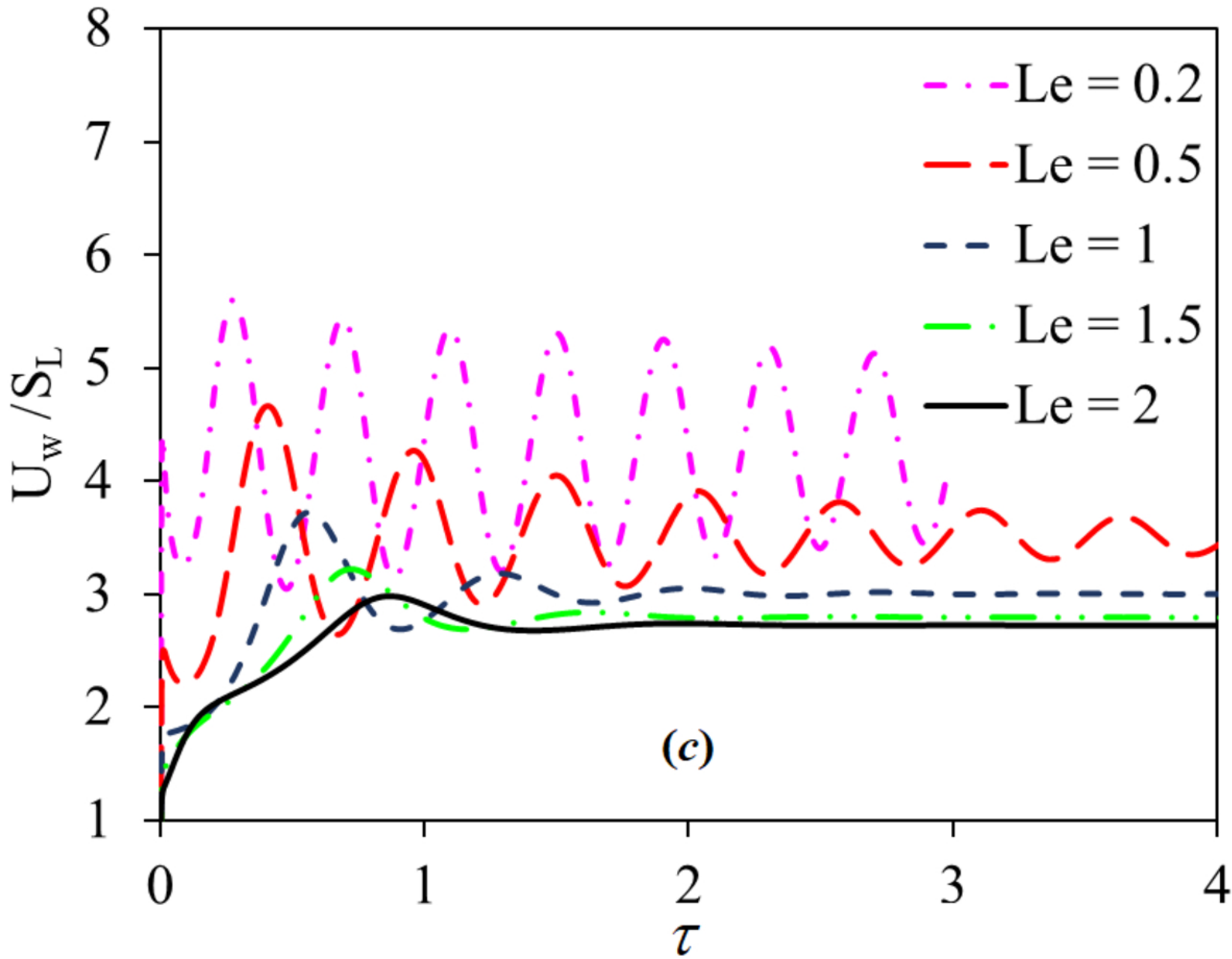


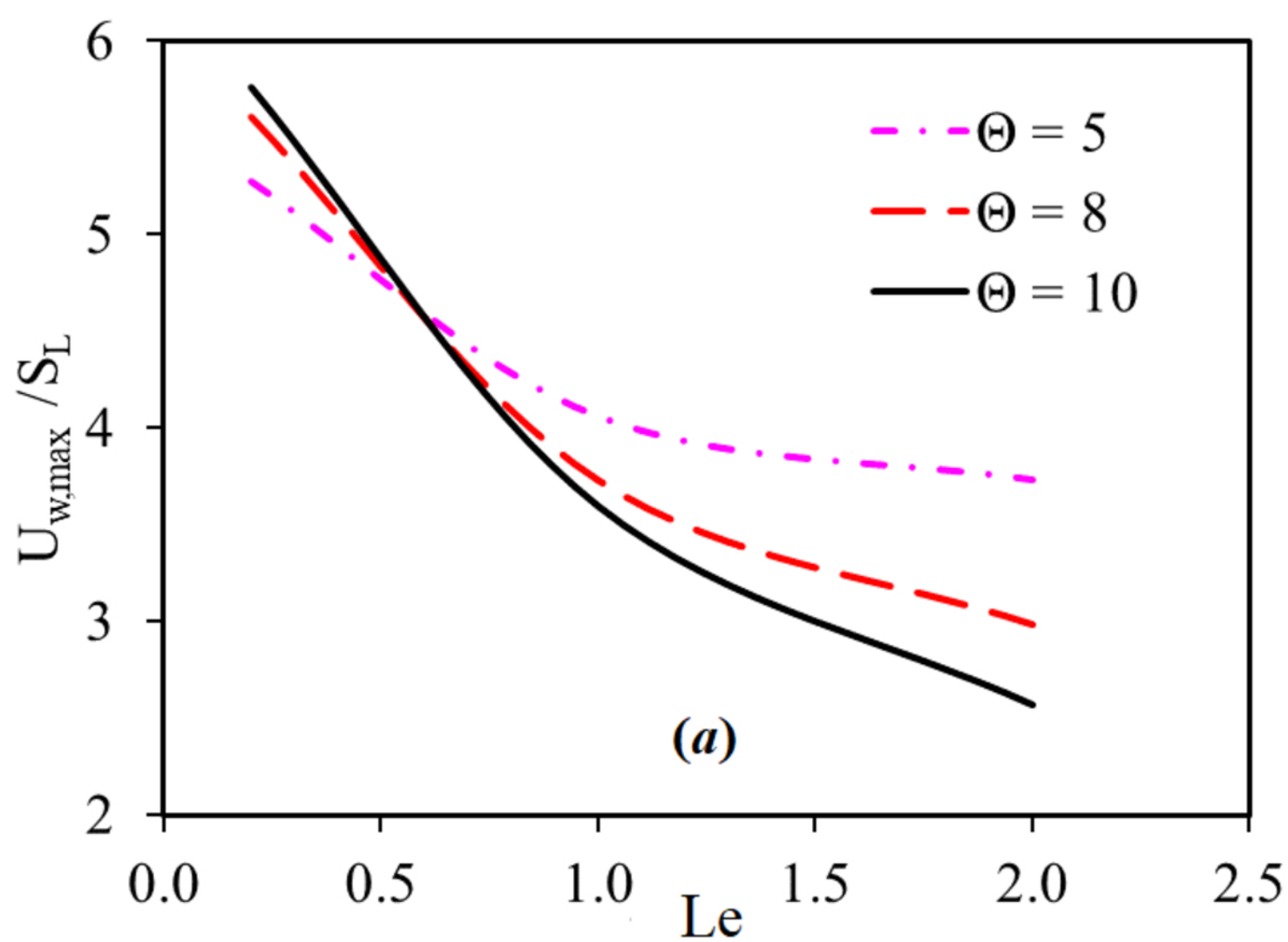


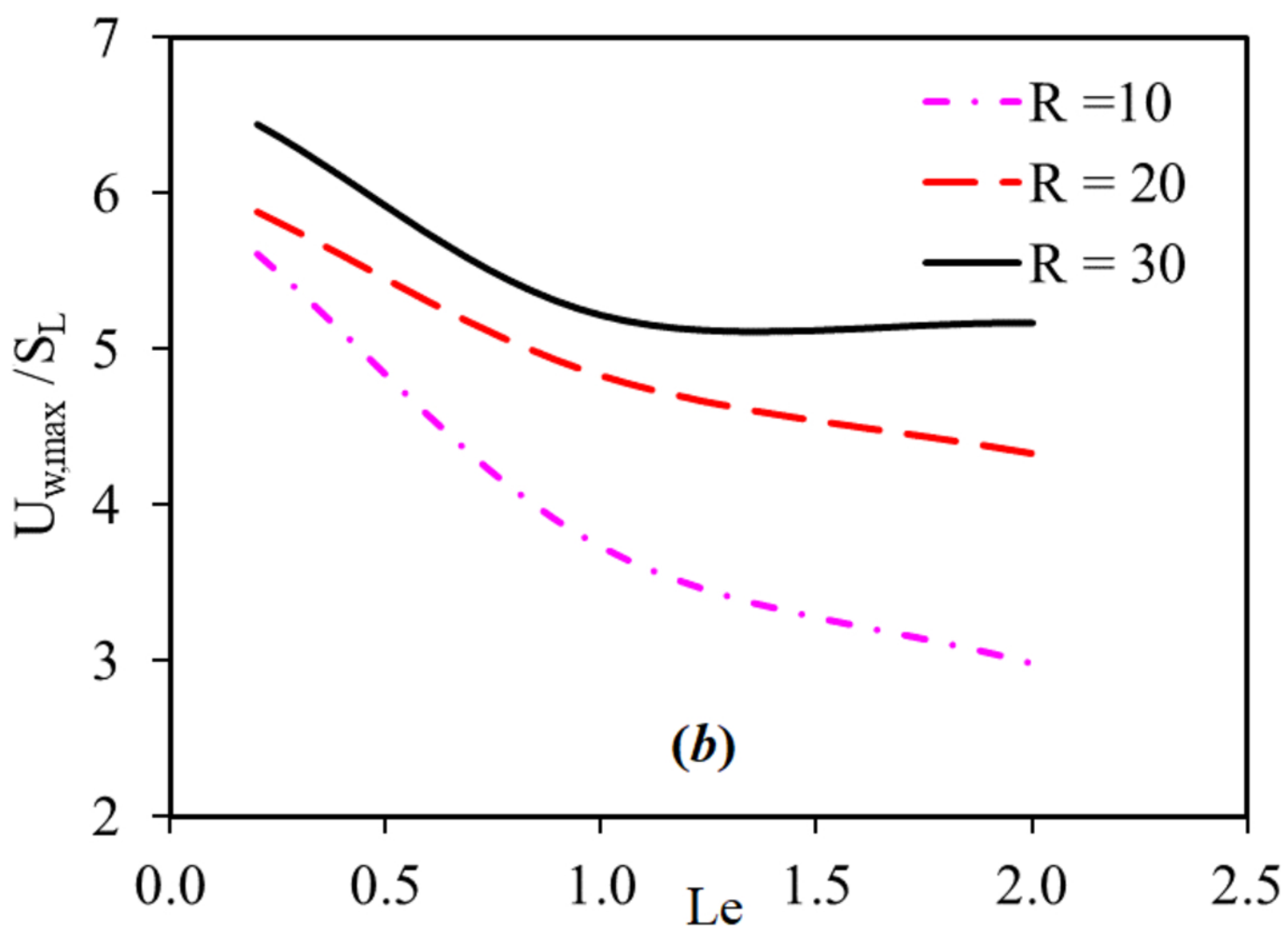












(a)

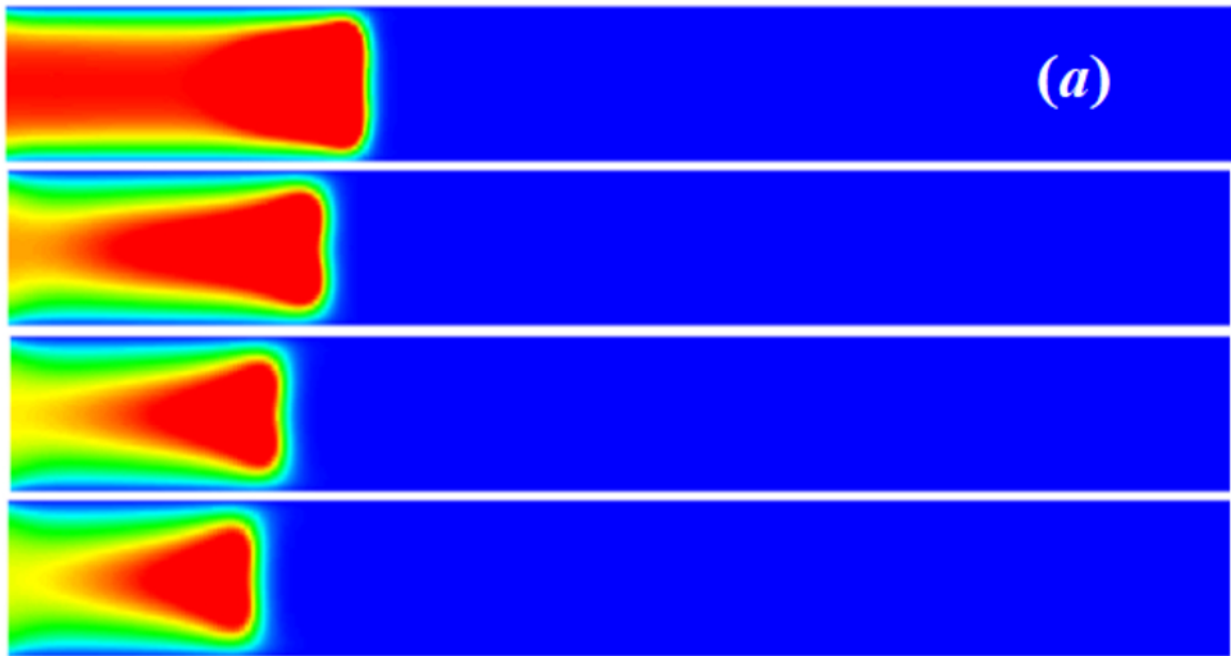
0

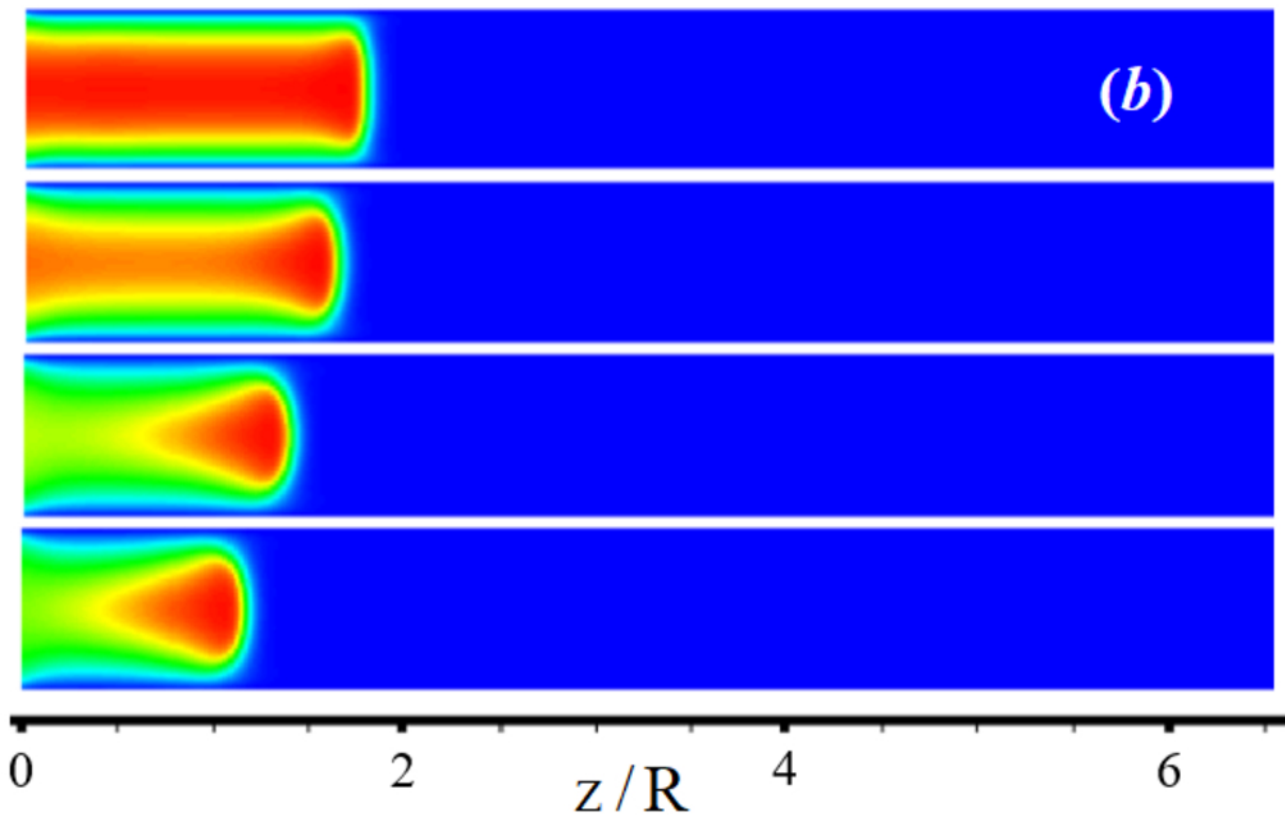
2

z/R

4

6





(c)

0

2

z/R

4

6

